NASA TECHNICAL MEMORANDUM

NASA TM X-62,348

NASA TM X-62,348

A STOL TERMINAL AREA NAVIGATION SYSTEM

Frank Neuman and David N. Warner, Jr.

Ames Research Center
Moffett Field, Calif. 94035

May 1974

TABLE OF CONTENTS

A STOL TERMINAL AREA NAVIGATION SYSTEM

Frank Neuman and David N. Warner, Jr.

Ames Research Center, NASA
Moffett Field, California 94035

ABSTRACT

This report describes the mechanization and performance of a STOL terminal area navigation system. The purpose of the navigation system is to allow flying with precision 4D-guidance along complex flight paths in the terminal area, and to develop requirements for STOL operations in the 1980s. Hence, the navigation aids include an experimental microwave landing system, MODILS.

The report is organized as follows: The systems description begins with the navigation aids. Then it is shown how the data are transformed and combined with other data to obtain position and velocity estimates. Also presented are some of the design changes and other features that were introduced as a result of flight testing. Next, the various ways of displaying navigation-derived data are given. Finally, simulator and flight test results are discussed.

INTRODUCTION

This report will describe the mechanization and performance of a STOL terminal area navigation system. Brief descriptions of the digital avionics system in which the navigation computations have been implemented are available in references 1 and 2.

The navigation system was specifically designed for use in the terminal area. The purpose of the navigation system is to allow the investigation of precision 4D guidance along complex flightpaths in the terminal area, and develop requirements for STOL operations in the 1980s. At that time microwave landing systems will be available. Hence, the navigation aids include an experimental microwave landing system, MODILS (ref. 3).

Because the navigation system described here is precise enough to permit 4D guidance of STOL aircraft along complex curved decelerating flightpaths, it will also be applicable to CTOL aircraft. In the 1980s, it is envisioned that ATC service will have increased ninefold over present service. To permit this large number of aircraft to be delivered to the runway with an accuracy of ±2 sec, as proposed in reference 4, a terminal area navigation system, which has increased precision as the aircraft approaches the runway, such as will be described in this report, will certainly be required.

The report is organized as follows: The systems description will begin with the navigation aids. Then it is shown how the data are transformed and combined with other data to obtain position and velocity estimates. In this section we will also present some of the design changes and other features that were introduced as result of flight testing. Next, the various ways of displaying navigation-derived data will be given. Finally, simulator and flight test results obtained in a Convair 340 will be discussed.

LIST OF ABBREVIATIONS

AHS	airborne hardware simulator
ATC	air traffic control
BCD	binary coded digit
CAT II	Category II landing weather minimum
CRT	cathode-ray tube
CTOL	conventional takeoff and landing aircraft
DME	distance measuring equipment
DR	dead reckoning
EADI	electronic attitude director indicator
FORTRAN	a high level computer language
HSI	horizontal situation indicator
ILS	instrument landing system
LGS	landing guidance system
MFD	multifunction display
MLS	microwave landing system
MODILS	modular instrument landing system
navaids	navigational aids
PCM	pulse code modulation
STOL	short takeoff and landing aircraft
STOLAND	trade name for the avionics system described in this report
TACAN	tactical air navigation
VOR	visual omnirange
VORTAC	collocated VOR and TACAN stations

3D	3 dimensional guidance (X, Y, Z)
4D	4 dimensional = 3D + time.

SYMBOLS

a_x, a_y, a_z	body axis accelerations
g	9.81 m/s^2
h_B	barometric altimeter altitude
h_R	runway altitude above mean sea level
h_{ref}	reference altitude
N	north
N_B	TACAN bearing bias error
N_m	magnetic north
R_s	(1) slant range from TACAN station, (2) slant range from MODILS azimuth antenna
s	LaPlace operator
V_T	true airspeed
X, Y, Z	actual aircraft position in runway coordinates (ft)
$\hat{X}$, $\hat{Y}$, $\hat{Z}$	estimated aircraft positions from complementary filters
$\dot{X}$, $\dot{Y}$, $\dot{Z}$	actual aircraft velocities in runway coordinates (ft/s)
$\hat{\dot{X}}$, $\hat{\dot{Y}}$, $\hat{\dot{Z}}$	estimated aircraft ground-speed components from complementary filters
$\dot{X}_A$, $\dot{Y}_A$	airspeed components in runway coordinates
$\hat{\dot{X}}_a$, $\hat{\dot{Y}}_a$	estimated true airspeeds in runway coordinate system
$\hat{X}_e$, $\hat{Y}_e$, $\hat{Z}_e$	position estimation errors $\hat{X} - X$, etc.
$\hat{\dot{X}}_e$, $\hat{\dot{Y}}_e$, $\hat{\dot{Z}}_e$	velocity estimation errors $\hat{\dot{X}} - \dot{X}$, etc.
X_R, Y_R, Z_R	raw, unfiltered navigation data
X_T, Y_T, Z_T	TACAN coordinates (ft)
$\hat{\dot{X}}_w$, $\hat{\dot{Y}}_w$	wind speed estimates in runway coordinate system
$\bar{X}_{\psi_M}$	MODILS azimuth and DME antenna X coordinates
X_l, Z_l	distance along and vertical to the 5° MODILS tilt plane
Y_E	MODILS elevation antenna Y coordinate

γ_I	inertial glideslope angle
γ_{ref}	reference glideslope angle
ε	total elevation angle of MODILS
ε_c	conical elevation angle of MODILS from 5° tilt plane
θ, ϕ, ψ	pitch, roll and yaw Euler angles
θ_E, ϕ_E, ψ_E	Euler angle measurement errors
θ_c	pitch command
ϕ_c	roll command
σ_ψ	standard deviation of the TACAN random heading error
σ_{ψ_B}	standard deviation of the TACAN bias error
$\psi = \psi_A - \psi_R$	runway referenced aircraft heading
ψ_M	aircraft conical azimuth angle from the centerline of the runway
$\psi_R = -7.3$	runway heading, from magnetic north (°)
ψ_T	aircraft bearing from TACAN station
ω_n	filter gains

NAVIGATION SYSTEM DESCRIPTION

Overview

Before going into details of the navigation system, a brief overview is given. As shown in figure 1, navaid position data as well as body accelerations are transformed to the local coordinate frame where they are filtered

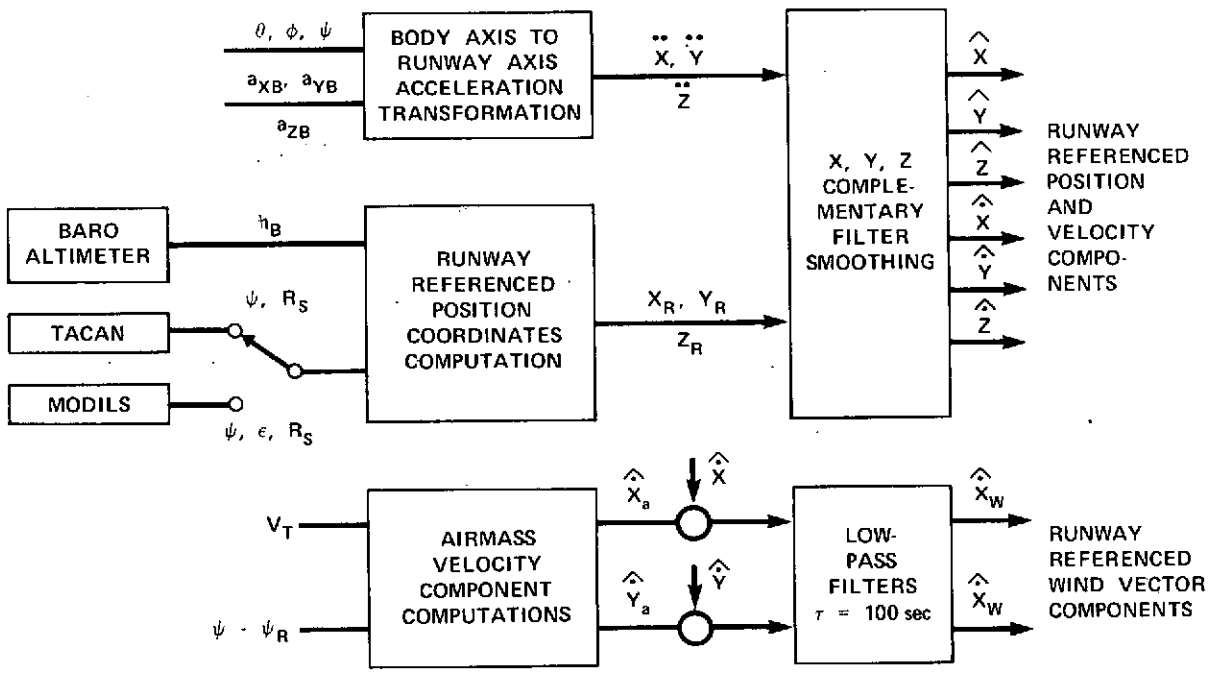

Figure 1.—Block diagram of navigation computations.

in separate X, Y, and Z complementary filters. The sensors used for navigation are the TACAN receiver and the scanning beam ILS receiver (MODILS), plus a body-mounted accelerometer package and the pitch, roll, and yaw angles from the attitude heading reference system as well as a barometric altimeter and an airspeed sensor. The navigation subroutines develop estimates of position and velocity with respect to the local coordinate frame which has its origin at the glideslope intercept point. In conjunction with air data, a wind vector is also estimated for use in the guidance computations. In case of navaid failure, the complementary filters are reconfigured for dead reckoning for a maximum of 2 min using air data and the last wind estimate.

The navigation concept was implemented on STOLAND, which is a flexible digital avionics research system. All calculations described here are performed in the STOLAND digital computer, which is a Sperry 1819A airborne digital computer, at a rate of 20 times per sec. For convenience, some calculations will be shown via their analog equivalents.

Coordinate System

Figure 2 is a map of the Crows Landing Test Facility, where the test flights are conducted. The coordinate system, which is also shown on this figure, has its origin at the center of the runway and the intersection of the perpendicular from the position of the MODILS glideslope to the runway centerline.

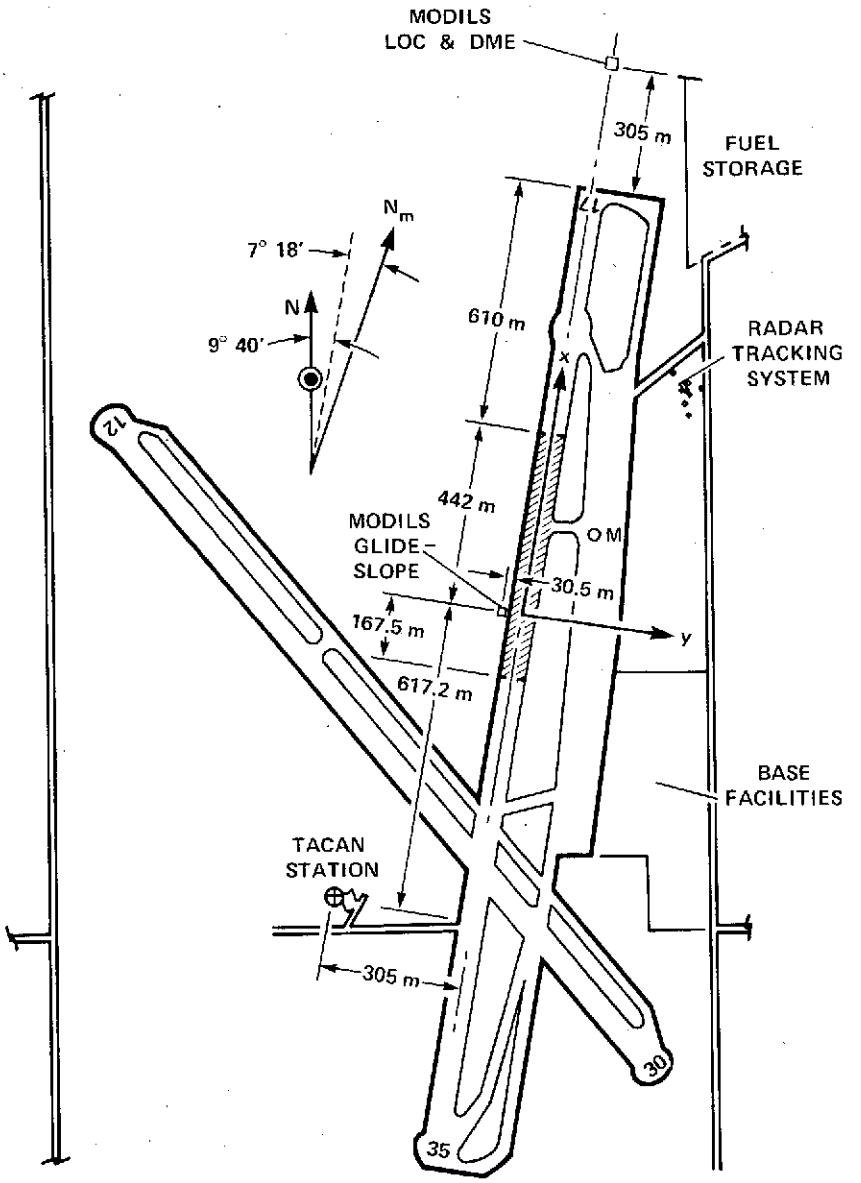

Figure 2.—Ground support equipment deployment at Crows Landing.

Two navigation aids shown in figure 2 are needed in the terminal area: One of moderate precision that covers a large area and one of high precision for approach and landing. Such navigation aids are provided at the Crows Landing test facility. The Crows Landing TACAN station and the MODILS scanning beam microwave landing system are the primary ground-based navigation aids for the terminal area navigation system.

For terminal area guidance, the local Crows Landing TACAN station must be chosen rather than a distant station. If this were not done, navigation errors for the terminal area would be too large, and the transition from TACAN to MODILS would cause large transients, which might force the automatic control system to disconnect.

Navaid Systems Equations and Data Quantization

For the navigation system design, the navaid data format must be known. All navigation data are ρ, θ data, which give position in terms of distances and angles. TACAN has cylindrical coordinates and MODILS a runway-oriented, conical coordinate system. Figure 3 shows the TACAN system coordinates as functions of the aircraft position.

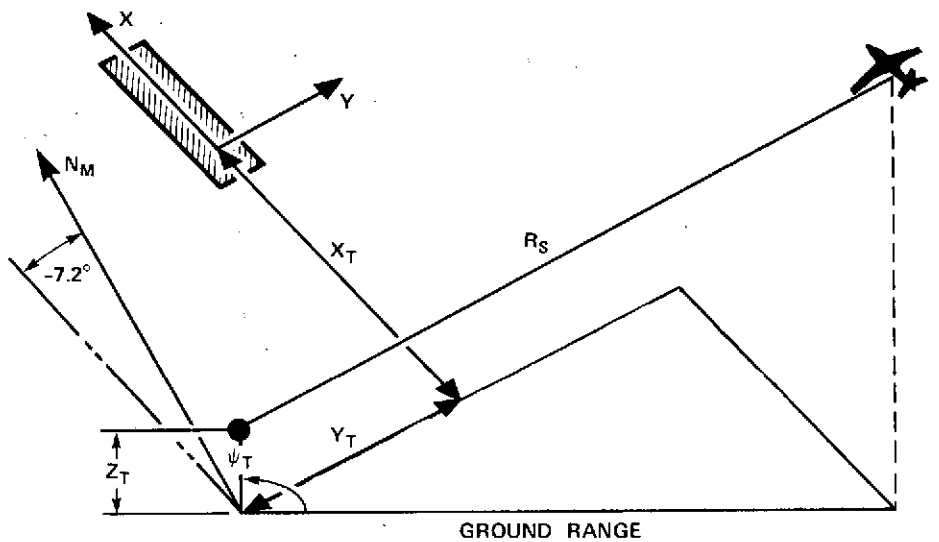

Figure 3.—TACAN coordinates.

The range is

$$R_S = \sqrt{(X - X_T)^2 + (Y - Y_T)^2 + (Z - Z_T)^2} \tag{1}$$

and the azimuth is

$$\psi_T = (\psi_R - 180) + 57.3 \tan^{-1}\left(\frac{Y_T - Y}{X_T - X}\right) \quad [°] \tag{2}$$

The navigation system transforms coordinates from the coordinate system of the selected navigation aid to the runway reference orthogonal coordinate system.

The solutions of the above equations for TACAN or VOR/DME and altimeter from cylindrical coordinates to the local earth reference frame have been mechanized in the Sperry 1819A airborne computer.

$$Z_R = h_B - h_R \tag{3}$$

$$X_R = X_T + \sqrt{R_s^2 - (Z_R - Z_T)^2}\cos(\psi_R - \psi_T) \tag{4}$$

$$Y_R = Y_T - \sqrt{R_s^2 - (Z_R - Z_T)^2}\sin(\psi_R - \psi_T) \tag{5}$$

where

h_R = 43 m, X_T = -785 m and Y_T = -305 m.

The subscript R has been added to the solution to indicate "raw" data which include noise.

The geometry of the MODILS system is shown in figure 4. Both antennas are conical scan antennas, the elevation antenna being tilted 5° above the plane of the coordinate system.

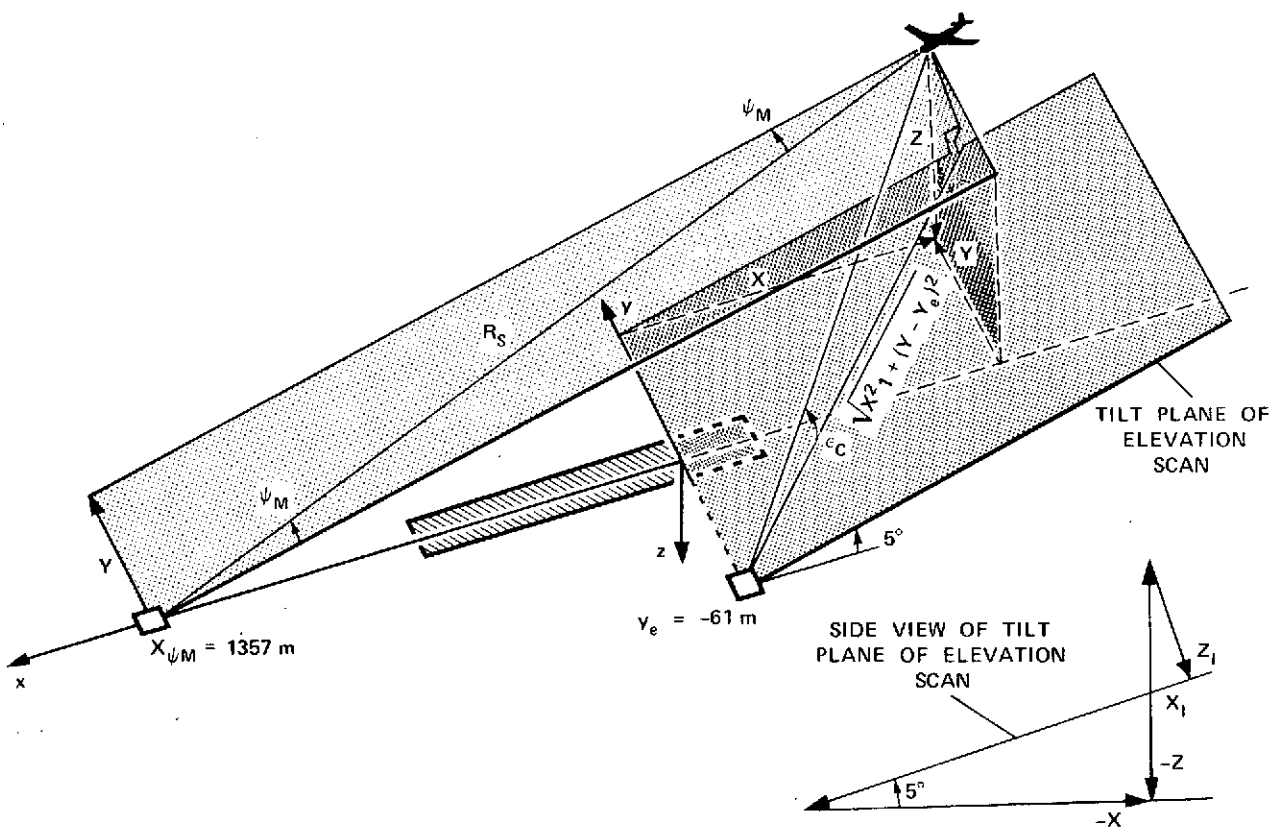

Figure 4.—Geometry of MODILS conical scan antennas using a runway-oriented coordinate system.

The cone of constant azimuth is obtained by swinging the triangle, which contains the DME line, around the y_{ac} axis shown in figure 4. The cone of constant elevation is obtained by swinging the triangle, which contains the angle ε_c as apex, on the 5° tilt plane with the apex fixed at y_E.

In terms of the chosen coordinate system, the MODILS equations are as follows:

Range:
$$R_s = \sqrt{(X_{\psi_M} - X)^2 + Y^2 + Z^2} \tag{6}$$

Azimuth:
$$\psi_M = \sin^{-1}\left(\frac{Y}{DME}\right) \tag{7}$$

Elevation:
$$Z_1 = (Z - X \tan 5°) \cos 5° \tag{8}$$

$$X_1 = X \cos 5° + Z \sin 5° \tag{9}$$

$$\varepsilon_c = \tan^{-1}\left(\frac{-Z_1}{\sqrt{X_1^2 + (Y - Y_E)^2}}\right) \tag{10}$$

$$\varepsilon = \varepsilon_c + 5° \tag{11}$$

Exact solution of the MODILS equations is impractical. The solution of the MODILS equations to runway reference coordinates from azimuth, elevation, and DME results is a fourth-order algebraic equation. It is quite lengthy to calculate the four coefficients in this equation and even more lengthy to calculate the four roots. Many test values were run on a general purpose computer, and it was found that two roots are always positive and can be discarded, since MODILS only covers the negative axis. However, the other two roots often have similar values and no simple criterion was found to select the solution that corresponded to the aircraft position. For these reasons, the method of calculating aircraft position from the two angles and DME has been abandoned and has been replaced by an approximate method.

The calculation of horizontal position coordinates from MODILS is accomplished by using azimuth and DME information in conjunction with pressure altimeter information.

$$Z' = h_B - h_R \tag{12}$$

$$Y_R = R_s \sin \psi_M \tag{13}$$

$$X_R = X_{\psi_M} - \sqrt{R_s^2 - Y_R^2 - Z'^2} \tag{14}$$

altitude calculations when inbound and less than 6 n. mi. from aiming point

$$\begin{cases} X_1 = X_R \cos 5° + Z' \sin 5° \\ Z_1 = -\sqrt{X_1^2 + (Y_R - Y_E)^2} \tan(\varepsilon - 5°) \\ Z_R = \dfrac{(Z_1 + X_R \sin 5°)}{\cos 5°} \end{cases} \tag{15}$$

altitude calculations outside MODILS elevation coverage

$$\{Z_R = -Z' \tag{16}$$

From the above equations, it can be seen that the calculation of X_R and Y_R is relatively insensitive to altitude errors. For most of the flightpath, the altitude measured by the pressure altimeter is used as altitude reference, since aircraft not equipped with computers fly to altimeter-referenced altitudes and all aircraft in a terminal area should be referenced to the same standard.

Once the horizontal position is calculated with the aid of the altimeter, a better altitude estimate can be obtained from the elevation scan angle, as shown above. Since 4D guidance usually ends in scanning beam LGS glideslope and localizer tracking, it is necessary to blend altimeter altitude into MODILS-derived altitude shortly before the final waypoint is reached in order to prevent a large altitude error at the final 4D guidance. The blending method and related problems are discussed in the subsection, "Altitude Blending."

The airborne system is digital; therefore, all angle and distance data are quantized. For VOR the sine and cosine of the bearing angle are received in the Sperry 1819A computer as two 12-bit words, which are derived in the data adapter by analog-to-digital conversion of the two-wire synchro outputs. The VOR/DME range is received as a digitally coded word where the least significant BCD digit represents 0.01 of a nautical mile (18.53 m). The TACAN receiver bearing and range outputs are both binary digital. The least significant bit in the range signal is 0.025 nautical mile (46.33 m) and is in the bearing signal 0.25°. The quantization for the scanning beam landing guidance system DME is one hundredth of a mile (18.53 m) for the least significant BCD digit. The MODILS azimuth is quantized to the nearest tenth of a degree and the elevation is quantized to the nearest one-hundredth of a degree. Both are received as BCD formatted data.

Inertial Measurements

Inertial measurements are required to smooth position and velocity data. The inertial measurements are the body axis accelerations measured with body-mounted accelerometers. Similar to the navigation aid data, the accelerations are transformed into runway-referenced acceleration components. This is done in two steps. First, the aircraft axis acceleration components are calculated:

$$\begin{bmatrix} \ddot{X}_{A'} \\ \ddot{Y}_{A'} \\ \ddot{Z}_{A'} \end{bmatrix} = \begin{bmatrix} \cos\theta & 0 & \cos\phi \sin\theta \\ 0 & \cos\phi & -\sin\phi \\ -\sin\theta & \sin\phi \cos\theta & \cos\phi \cos\theta \end{bmatrix} \begin{bmatrix} a_x \\ a_y \\ a_z' \end{bmatrix} + \begin{bmatrix} 0 \\ 0 \\ g \end{bmatrix} \tag{17}$$

The above calculations are explained as follows. In accelerometer packages, it is standard practice to electrically bias the normal accelerometer with a signal of -1 g so that in level, unaccelerated flight, the accelerometer output will be very small, and the output can be used directly for simple autopilot control systems.

But the accelerations are made with respect to the runway-oriented coordinate system. Hence, first, the electrical bias of 1 g in the Z accelerometer is removed by subtracting 1 g from the accelerometer reading $a'_z = a_z - g$. Second, the measured accelerations are transformed into a horizontal level aircraft axis coordinate system via the measured Euler angles θ, ϕ, ψ. If the aircraft were in unaccelerated flight, the measured vertical component of acceleration would be -1 g due to the gravitational field; hence, 1 g is added to the Z acceleration component. As a second step, the inertial acceleration components are transformed into the runway coordinate reference system:

$$\begin{bmatrix} \ddot{X}_R \\ \ddot{Y}_R \end{bmatrix} = \begin{bmatrix} \cos\psi & -\sin\psi \\ \sin\psi & \cos\psi \end{bmatrix} \begin{bmatrix} \ddot{X}_{A'} \\ \ddot{Y}_{A'} \end{bmatrix} \tag{18}$$

$$\ddot{Z}_R = \ddot{Z}_{A'} \tag{19}$$

At this point, both position data and inertial data are in the runway reference coordinate system and can be applied directly to the complementary filters. The filters will be described next.

Complementary Filters

After coordinate transformation, the navigation data are combined in complementary filters. Figure 5 shows the complementary filters that are presently implemented. The complementary filters for the horizontal coordinates are standard, third-order filters.

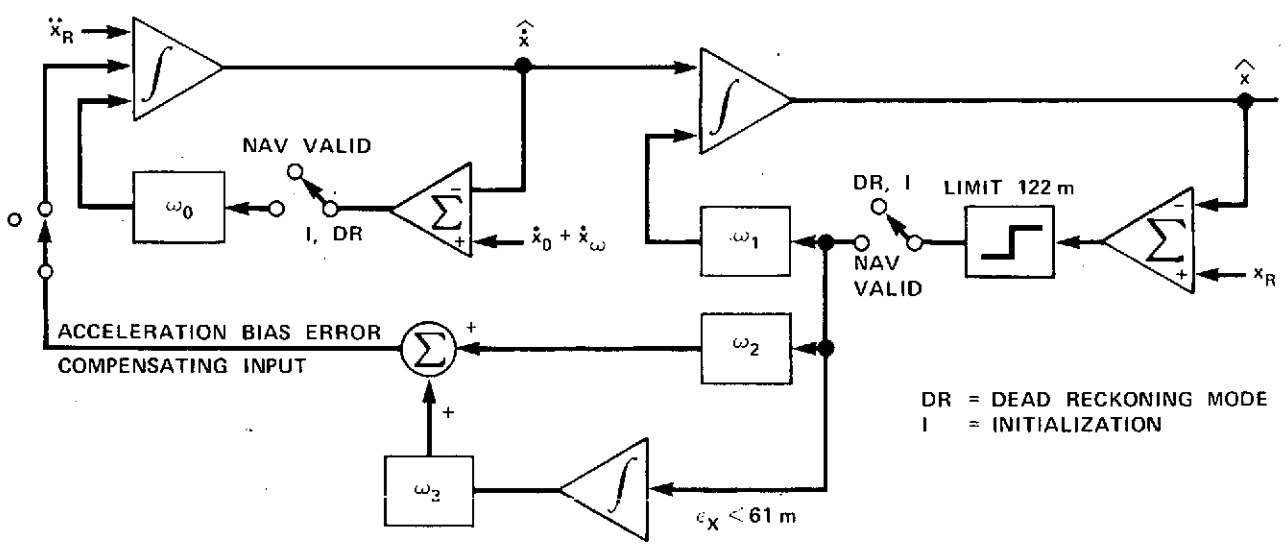

Figure 5a.—Third-order filter for $\hat{X}$ and $\hat{Y}$, $\hat{\dot{X}}$, $\hat{\dot{Y}}$ estimates.

The transfer functions for both the velocity and position estimates are:

$$\left.\frac{\hat{X}(s)}{\ddot{X}_R(s)/s^2}\right| = \frac{s^3}{s^3 + \omega_1 s^2 + \omega_2 s + \omega_3} \quad (20) \qquad \left.\frac{\hat{\dot{X}}(s)}{\ddot{X}_R(s)/s}\right| = \frac{s^3 + \omega_1 s^2}{s^3 + \omega_1 s^2 + \omega_2 s + 1} \quad (21)$$

$$X_R^1 = 0 \qquad X_R = 0$$

$$\left.\frac{\hat{X}(s)}{X_R(s)}\right| = \frac{\omega_1 s^2 + \omega_2 s + \omega_3}{s^3 + \omega_1 s^2 + \omega_2 s + \omega_3} \quad (22) \qquad \left.\frac{\hat{\dot{X}}(s)}{X_R(s)\cdot s}\right| = \frac{\omega_2 s + \omega_3}{s^3 + \omega_1 s^2 + \omega_2 s + 1} \quad (23)$$

$$\dot{X}_R = 0 \qquad \ddot{X}_R = 0$$

The presence of the LaPlace operator on the left side of the equations for either integration or differentiation results in transfer functions that are ratios of filtered to nonfiltered estimates of position or velocity from measurement of acceleration or position. For both estimates, the sums of the transfer functions for velocities [(21) plus (23)] and positions [(20) plus (22)] are equal to 1. This means that, if both inputs to the filters are error-free, the resulting outputs will be error-free and free of any dynamics of the filter. The nominal filter gains are:

$$\omega_0 = 0.2, \quad \omega_1 = 0.2, \quad \omega_2 = 0.015, \quad \omega_3 = 0.0005$$

These gains give smooth position and velocity estimates within 10 n. mi of the navigation aids. There are two drawbacks to constant gain filters. First, at large distances from the navigation aids, the filtered outputs are too noisy for smooth guidance unless the guidance gains are reduced as a function of distance. As a better solution, one relies more heavily on the inertial data and reduces the navigation filter gains. Secondly, although the noise for the nominal filter gains in the vicinity is quite low, a step bias error of $\ddot{X} = 0.3$ m causes maximum transient position and velocity errors of 16.1 m and 3.35 m/sec errors, which do not damp out to 10% of the maximum values for 70 sec. As discussed later, such errors do occur after tight turns and cause crosstrack guidance errors that are serious when the turn is followed by a 1 min final approach. The solution was to increase the filter gains to $\omega_1 = 0.8$, $\omega_2 = 0.24$, $\omega_3 = 0.032$ when in MODILS coverage and when the distance to touchdown is less than 6 n. mi. With these gains for the same step bias error, the transient errors reach maxima of 1 m and 0.85 m/sec and are damped out to less than 10% of the maximum values after 16 sec. The cost of decreasing the effect of bias errors is some increase in higher frequency noise. In future navigation systems (to be installed in the Augmentor Wing Research Jet Aircraft and Twin Otter) the filter gains are made continuously variable.

The vertical position and speed are estimated by a second-order complementary filter (figure 5b).

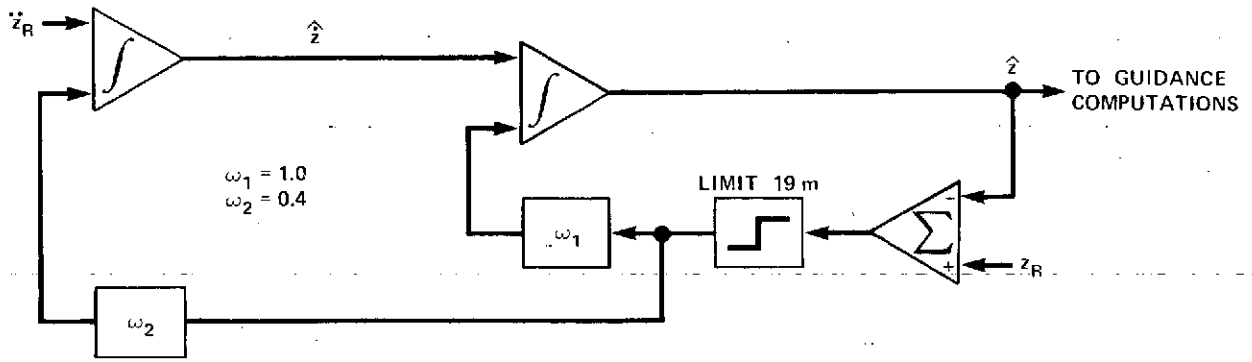

Figure 5b.—h filter.

The transfer functions of the altitude estimation filters are:

$$\left.\frac{\hat{Z}(s)}{\ddot{Z}_R(s)/s^2}\right| = \frac{s^2}{s^2 + \omega_1 s + \omega_2} \quad (24) \qquad \left.\frac{\hat{\dot{Z}}(s)}{\ddot{Z}_R(s)/s}\right| = \frac{s^2 + \omega_1 s}{s^2 + \omega_1 s + \omega_2} \quad (25)$$

$$\ddot{Z}_R = 0 \qquad Z_R = 0$$

$$\left.\frac{\ddot{Z}(s)}{Z_R(s)}\right| = \frac{\omega_1 s + \omega_2}{s^2 + \omega_1 s + \omega_2} \quad (26) \qquad \left.\frac{\hat{\ddot{Z}}(s)}{Z_R(s)\cdot s}\right| = \frac{\omega_2}{s^2 + \omega_1 s + \omega_2} \quad (27)$$

$$\dot{Z}_R = 0 \qquad \ddot{Z}_R = 0$$

For the second-order filter, a bias error in the accelerometer will result in a constant speed and position error.

The filters must be protected against large input errors. Due to the digital nature of the signals, momentary signal dropouts or errors in a single bit can cause extremely large momentary measurement errors. When such errors are applied to an unprotected filter, large transients will occur at the filter output. These transients are prevented by limiters shown in figures 5a and 5b which are placed after the summing junction of the estimated minus the measured position.

Dead Reckoning (DR) Computations

The computation of components of velocity relative to the airmass are:

$$\hat{\dot{X}}_A = \left|V_T^2 - (\dot{Z}_R)^2\right|^{\frac{1}{2}} \cos \psi \quad (28)$$

$$\hat{\dot{Y}}_A = \left|V_T^2 - (\dot{Z}_R)^2\right|^{\frac{1}{2}} \sin \psi \quad (29)$$

where $\dot{X}_A$, $\dot{Y}_A$ = airspeed components in the coordinate system

V_T = true airspeed

$\dot{Z}_R$ = smoothed vertical speed

ψ = aircraft heading (runway reference) = $(\psi_A - \psi_R)$

During the DR mode the airspeeds $(\hat{X}_A, \hat{Y}_A)$ and $(\hat{X}_w, \hat{Y}_w)$ are switched into the complementary filter for velocity determination in that mode (see figure 5b); the values $(\hat{X}_w, \hat{Y}_w)$ are taken to be the same as the values computed prior to switching into the DR mode. To prevent frequent transients from switching between navaids, when MODILS valids are lost in automatic navigation, the system will go to dead reckoning for 2 sec before switching to TACAN. When all navaids are invalid, the system will continue in the dead reckoning mode for 2 min.

Other Features of the Navigation System

Automatic Navaid Switching. The software is programmed to select automatically receiver outputs from the TACAN receiver tuned to the Crows Landing Station and the MODILS receiver, if the pilot selects this option. Navaids are selected such that the most accurate navaid is chosen first. The inverse order of accuracy is MODILS, TACAN, and dead reckoning. As discussed later, switching between navaids causes transients in both position and velocity estimates. Therefore, switching must be avoided as much as possible. Since, at the entrance into the MODILS region, the MODILS signal may become valid and invalid several times before settling down, the nav-valids are accepted in the proportional signal region only. The automatic navigation routine also checks if the pilot has selected the TACAN radial tracking autopilot mode. In this case, automatic navaid switching is inhibited.

Navaid Valids. Navaid valids alone do not guarantee good navigation data. Valids are discrete electrical signals from navigation receivers that indicate reasonable signal strength or, in the case of DME, signal lock. For TACAN and VOR stations, there exists a 60° cone of confusion, where the azimuth data are erratic. For the MODILS system angle information, there exists a range of proportional signals that is smaller than the valids would indicate. Therefore, the navigation valids are set to be invalid if (1) the aircraft is within the cone of confusion for TACAN, (2) if the MODILS azimuth is outside ±20°, (3) if the MODILS elevation is outside 2 to 15°, or (4) if the MODILS DME is less than 300 m.

Navaid Switching Transient Reduction. When switching between two navaids that give different position information due to bias errors, a position estimation transient cannot be avoided. However, bias errors alone result in small errors of velocity estimates. Therefore, to avoid large velocity estimate transients after navaid switching when the position estimate changes rapidly, the feedback loop called "acceleration bias error compensation" in figure 5a input is opened for 15 sec after switching.

Enroute Navigation. For pilot convenience, limited enroute navigation capability from Moffett Field to Crows landing is provided. For enroute navigation, the coordinates of the Moffett Field TACAN station, the San Jose VOR station, and the Stockton and Oakland VORTAC stations are stored in the computer and are properly entered into the calculations upon keyboard selection by the pilot. No automatic receiver tuning is provided. The pilot must tune the proper station and enter a mnemonic into the keyboard to indicate to the STOLAND navigation system which VOR or VORTAC station is tuned.

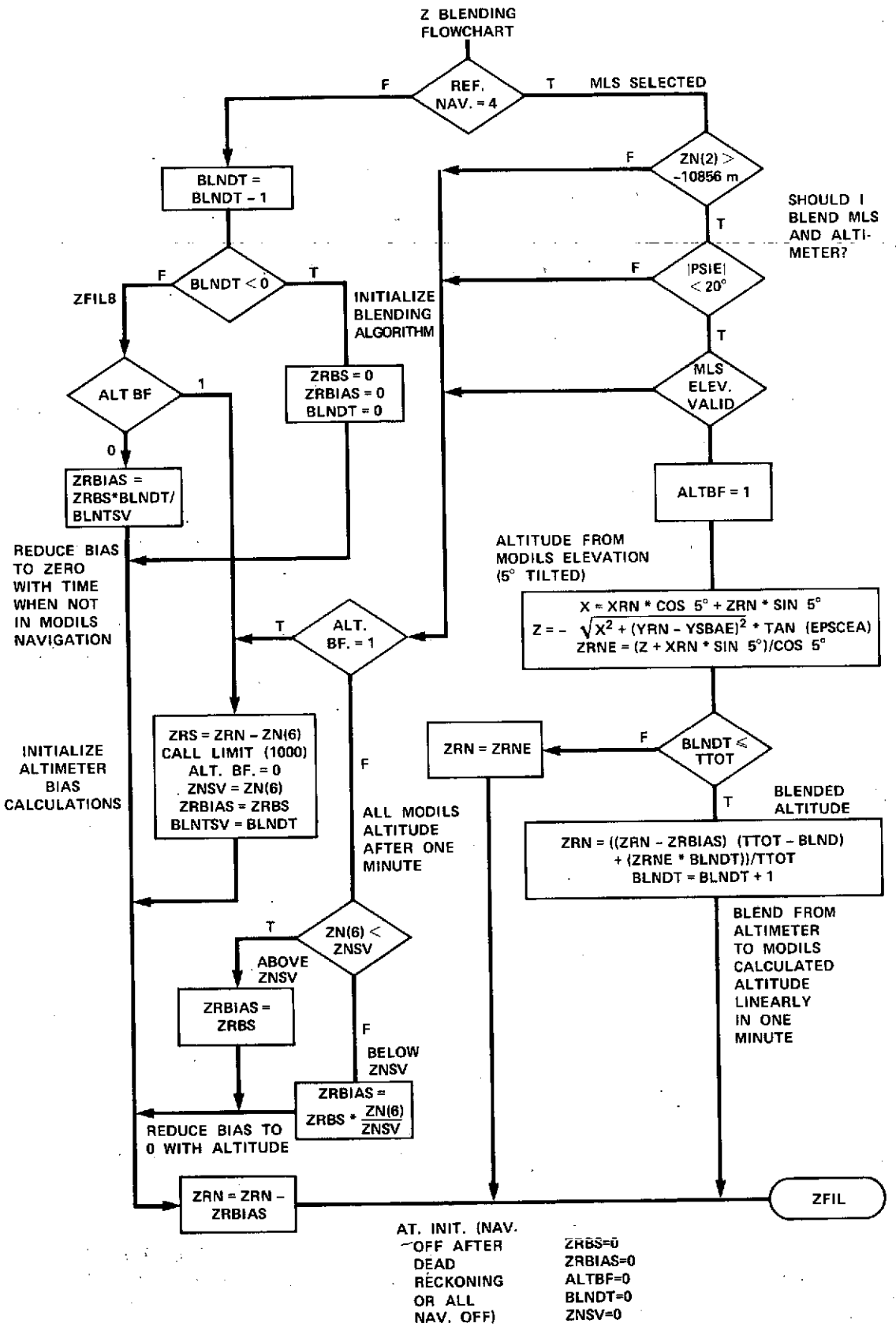

Figure 6.—Z-blending flowchart.

(see next page for explanation of symbols)

ALTBF	test flag for first time out off elevation scan altitude computations
BLNDT	60-sec counter
TTOT	60*20 intervals
ZRNE	altitude from SBILS
ZRN	input: raw altimeter altitude
	output: raw blended altitude
ZNSV	save filtered altitude at time of switching to altimeter from SBILS
ZRBIAS	altimeter bias at time of switching to altimeter from SBILS
ZRBS	altimeter bias initialization

Prevention of Filter Lockouts. It is possible that large temporary navigation errors from the receivers which are not detected by loss of signal valids cause the raw and filtered estimates of position to differ by a value greater than the limiter value in the X and Y position filters. When this happens, the filters might never reconverge to the proper position estimates. Therefore, if the limiters are saturated for more than 15 sec, we return to a filter convergence routine (initialization). Also, if for any computation cycle the difference between raw and filtered estimates of position differ by more than 1000 m, we use the dead reckoning mode for that cycle. However, if such error exists consecutively for more than 15 sec, we also return to the filter initialization routine.

Altitude Blending. To prevent abrupt dives or climbs of the airplane when switching vertical navigation sources, some form of signal blending is required. Upon entry into the MODILS signal area, the chosen blending algorithm linearly weights MODILS and altimeter-derived altitudes in such a manner that, after 1 min, altimeter altitude is not used at all and MODILS derived altitude is used altogether. Due to the possibility of signal dropouts, this requires the somewhat complicated program that is illustrated in figure 6. Blending will take place only if the MODILS system is selected; it will start when the aircraft is less than 6 n. mi. from the runway, when the heading is toward the runway, and when the MODILS elevation is valid. Blending is stopped when any of these conditions become invalid. When blending is stopped, the altimeter alone will be used as the altitude reference, except for a constant value, the difference of the last estimated altitude from MODILS and present altimeter reading, which is added to prevent an altitude transient. During absence of the MODILS elevation valid, this constant is linearly reduced with altitude to 0 at runway altitude, since it is assumed that the altimeter has been properly referenced to the barometric pressure of the runway. (For an operational Microwave Landing System, elevation signals may seldom be lost during approaches and one might dispense with this programming complexity.) If a go-around is performed, the system will go off MODILS navigation and the altimeter bias will be removed as a function of time in about 1 min.

When two altitude estimates are combined as input to a complementary filter, the altitude and the rate outputs will be in error during the time of blending. When the altitude error is not too large, this effect may be desirable. Assume a tight control system with a control law of the form

$$\theta_c = K_1 h_{error} + K_2 (\gamma_I - \gamma_{ref}) \tag{30}$$

where

$$\gamma_I = \dot{h}/v_{ground} \tag{31}$$

Figure 7 shows paths that would be flown if the system had an initial barometric altitude error which is reduced in 1-min intervals to the smaller MODILS altitude error. Both the calculated h_{error} and $-h_{ref}$ would be 0 along these paths, and the path indicated on the EADI in terms of flight director bar and ILS window position would be the nominal paths.

Figure 7 includes a simulator trace of the actual flight paths for an automatic flight when an altimeter error of about 61 m exists at the initial blending altitude.

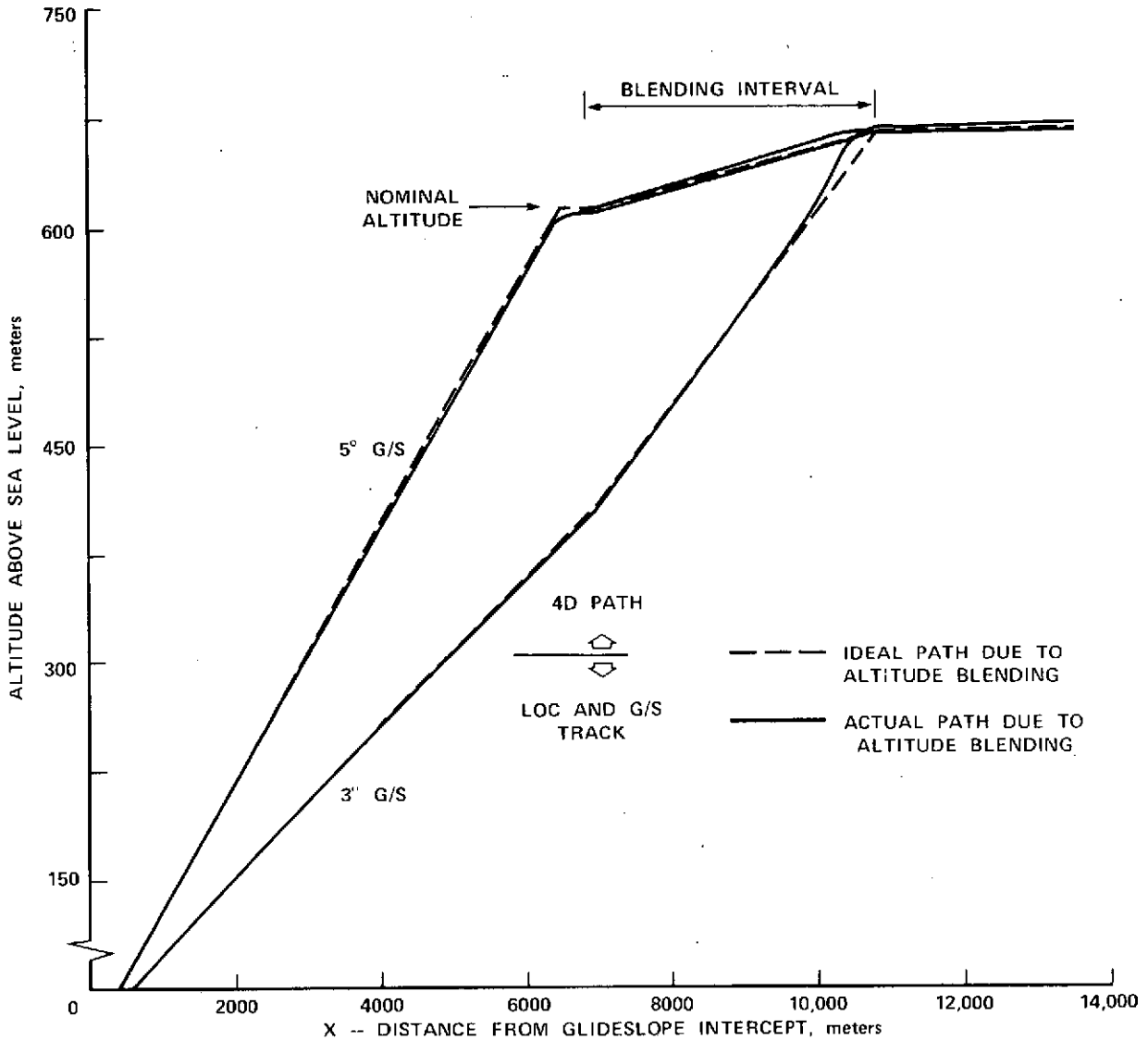

Figure 7.—Effect of altitude blending on automatic flight.

NAVIGATION SYSTEM SENSORS

The navigation system includes various sensors which provide radio, inertial, and air data information used for 3D and 4D navigation computations. A listing of these sensors appears below. Pertinent signal and power details appear on data sheets in appendix II.

- TACAN receiver/transmitter
- DME distance measuring equipment
- VOR/ILS receiver
- Radio altimeter
- MODILS
- Pitch rate gyro
- Yaw/roll rate gyro
- 3-axis accelerometers
- Static pressure sensor
- Differential pressure transducer
- Total temperature sensor
- Vertical gyro

DISPLAY OF NAVIGATION DATA

Overview

STOLAND includes a sophisticated computer-driven display system on which navigation and other data are displayed. The navigation data are displayed on three display units: the Electronic Attitude Director Indicator (EADI), the Horizontal Situation Indicator (HSI), and the Multi-Function Display (MFD). Navigation data are also used internally in the system for conventional guidance modes and for 4D guidance. This subject will be treated elsewhere. The various displays and navigation data processing will be discussed next.

Electronic Attitude Director Indicator (EADI)

Several symbols on the electronic attitude director are devoted to the display of processed and unprocessed navigation data. In the upper center is a programmable numerical display, which can display altitude rate, flightpath angle, and distance to touchdown. Figure 8 also shows a symbolic display of

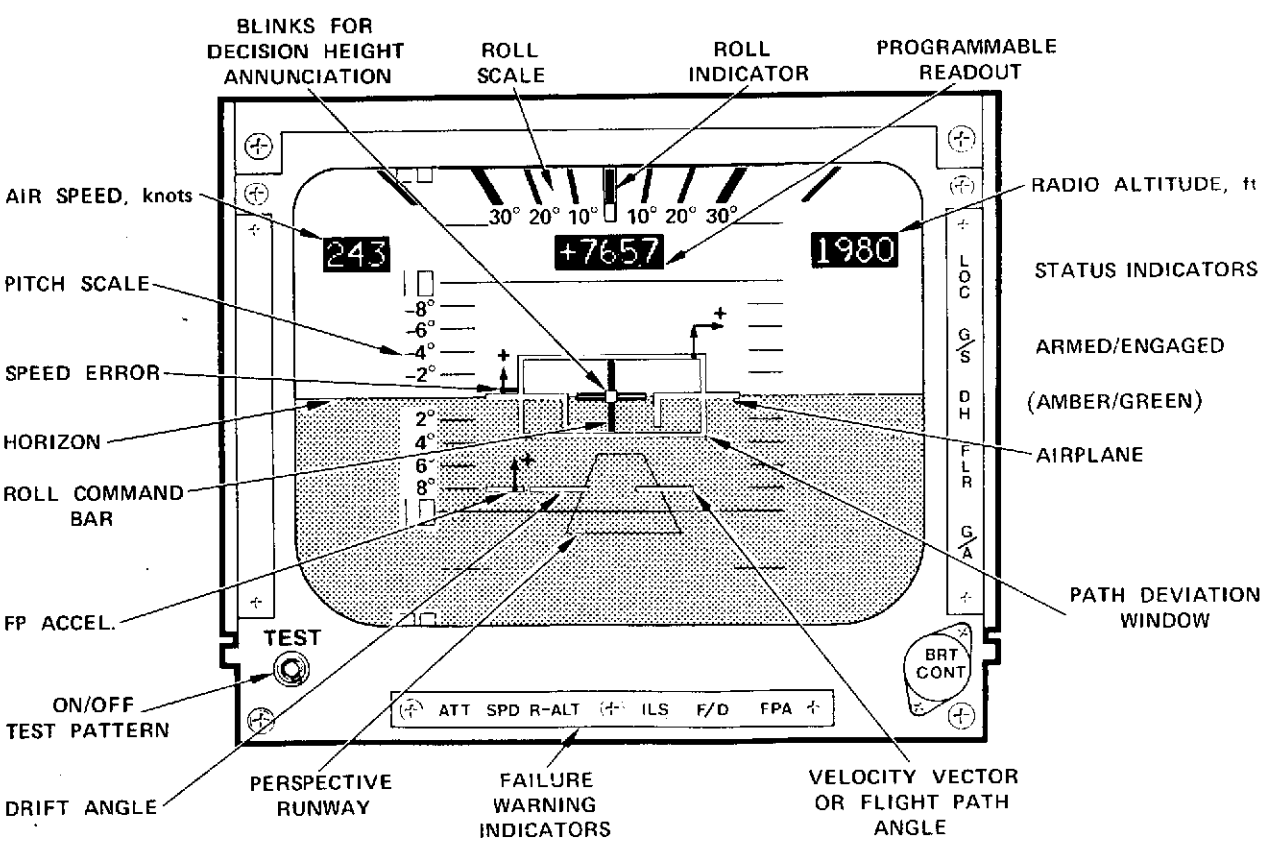

Figure 8.—Electronic attitude director indicator.

the flightpath angle during flight in the MODILS region, where navigation is accurate and the flightpath angle bar is split into two bars. In the MODILS region, the lateral deflection of the flightpath angle bar represents the drift angle. This is essentially a velocity vector presentation, which is derived from the velocity estimates of the navigation filters. In the TACAN region, the flightpath angle bar is a centered single bar, since drift angle information is not available.

A symbol that is derived from the position data is the perspective runway display. This is a true perspective display of the runway, as if the pilot's eye were 23 cm away from the display. The viewing distance has been chosen in such a manner that the velocity vector display will coincide with the front edge of the runway display during the approach. The front edge of the runway display is a line that contains the aiming point and does not represent the runway threshold. Flight experience has shown that this display gives a realistic representation of the outside world; however, no extensive evaluation of the usefulness of these symbols has been made as yet. It also should be noted that this is not a separate landing monitor, since the symbol position and movement are controlled by primary navigation data. The runway display contains coordinate transformations as well as a windowing program. The execution time required is 3.9 msec for the runway display and 1.1 msec for the rest of the EADI program.

Another navigation display is the path deviation window. This window displays angular deviation data in ILS approaches or scanning beam LGS approaches. During flight in the 4D guidance mode along complex curved paths, this window displays deviations from the reference flightpath. The overall philosophy for this display is described next.

The path deviation window on the EADI is used to display flightpath error quantities. The vertical dimension of one half is 1.13 cm and the horizontal dimension of half the window is 2.53 cm. The window is programmed as a tube that the aircraft is to fly through. For ordinary ILS, the sensitivity of this window has been set so that the outer edges are at the edges of the CAT II windows. For STOL approaches combined with 4D guidance along a predetermined path, the situation is more complicated. The sensitivities for localizer and and glideslope tracking should be dependent on glideslope angle and on the position of the final 4D guidance waypoint. If a constant angular sensitivity of the window were kept as in ILS, there would be a jump of the window at the transition from 4D guidance to glideslope and localizer tracking. This would be equivalent to a sudden constriction or increase of the size of the tube through which the pilot must guide the aircraft in order to meet the proper touchdown conditions.

It is undesirable to have any jumps in the window and a continuous tube is presented as shown in figure 9. The lateral deviation for the 4D guidance portion of the flightpath for half a window at present has been chosen to be 152.4 m (figure 9a). The final waypoint of the 4D path is on the center of the glideslope and localizer beams for the selected glideslope reference. For the specific MODILS azimuth antenna location with respect to the STOL runway threshold, it was decided to use a lateral angular sensitivity of 1° for half the window width below 91 m in altitude, and at higher altitudes, an angular sensitivity such that the half-window deviation matches the half-window deviation for the 4D guidance portion of the path at the final waypoint.

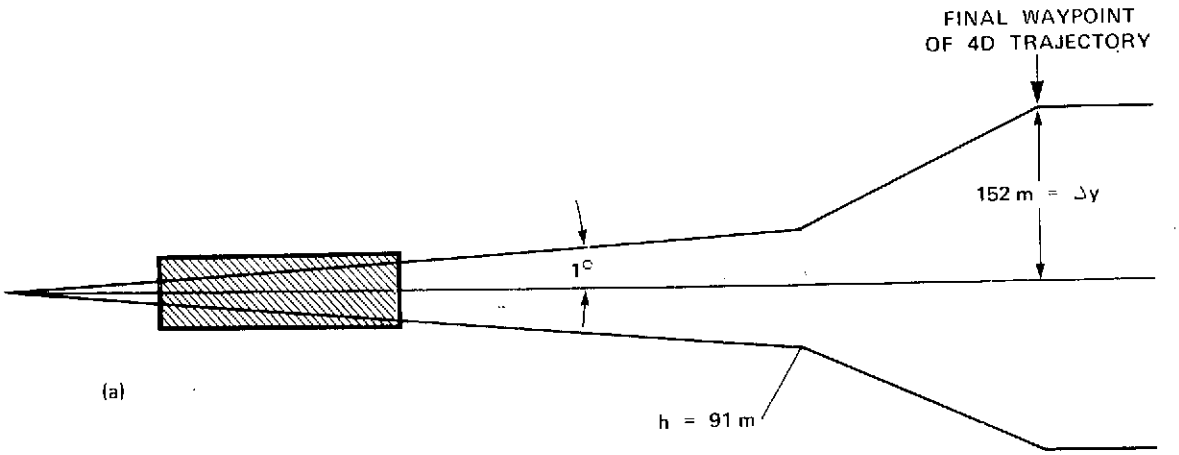

(a) Lateral window dimensions.

Figure 9.—Flightpath window sensitivities (not drawn to scale).

The glideslope error display (that is, the vertical motion of the path deviation window) is handled in a similar manner (figure 9b). Again, there must be no jump in the window; that is, no discontinuity in the tube that the aircraft must fly through. For the reference flightpath, an altitude error of ±15.24 m has been chosen to represent one-half window deflection. At the final waypoint, this is changed to an angular error display in such a manner that on the transition at the final waypoint to glideslope tracking the angular error corresponds to 15.24 m. A displacement due to altitude error will be calculated simultaneously with 3.66 m corresponding to one-half window, and the smaller displacement will be displayed. Category II requirements for CTOL aircraft state that the aircraft must stay within ±3.66 m of the glideslope from an altitude of 91 m down or go-around. Therefore, the tube must be narrowed to ±3.66 m at an altitude of 91 m or above. If calculations show that the final waypoint has been chosen too close to touchdown so that the 3.66 m tube begins at an altitude below 91 m, an error message to that effect will be displayed to the pilot. Window displacement gain calculation require as input only the coordinates of the final waypoint.

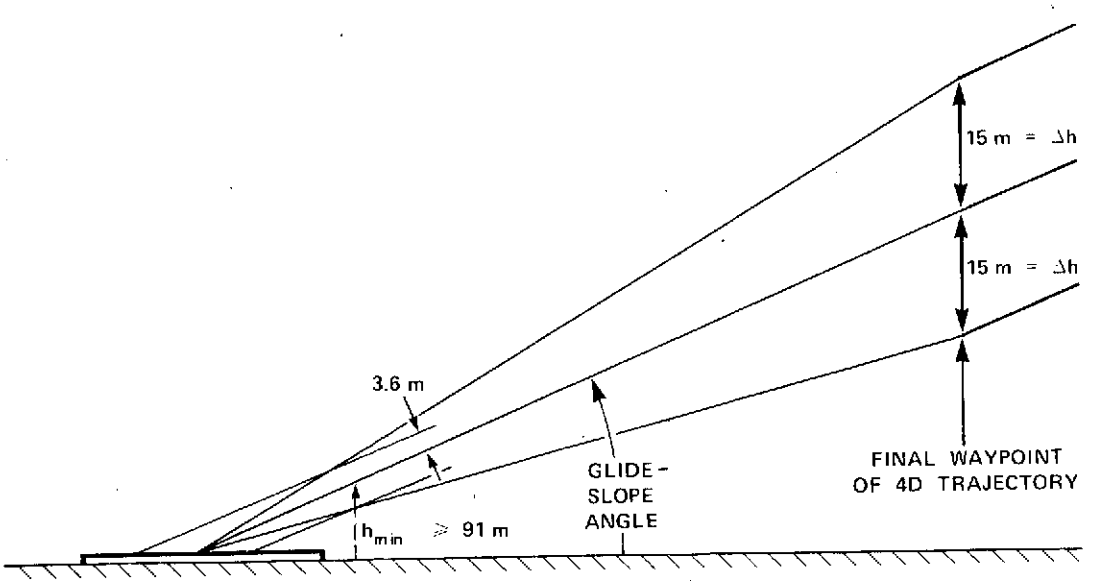

(b) Vertical window dimensions.

Figure 9.—Concluded.

Horizontal Situation Indicator (HSI)

Raw and processed navigation data are shown on the horizontal situation indicator (see figure 10). When STOLAND is operating on a programmed flightpath, the glideslope and course deviation indicators automatically show deviation from that flightpath as long as valid data are available. Raw data from the navaid receivers are provided to the HSI at all times. The number 1 distance window and bearing pointer show distance and bearing to either the VOR/DME station or MLS azimuth transmitter selectable by a switch on the left of the instrument. The number 2 distance window and bearing pointer show distance and bearing to either TACAN or the next waypoint of the programmed flightpath, as selected by a switch on the right side of the instrument. The gain of the glideslope deviation pointer is chosen as an inverse function of the glideslope reference angle so that, for a given altitude, the deflection is proportional to the altitude error. The nominal gain is the standard one for a 2.75° ILS glideslope, which is 0.35° for one dot. The nominal gain on the course deviation bar is 1° for one dot. On the programmed flightpath, the one dot glideslope and course deviation bar are 154 m and 381 m, respectively.

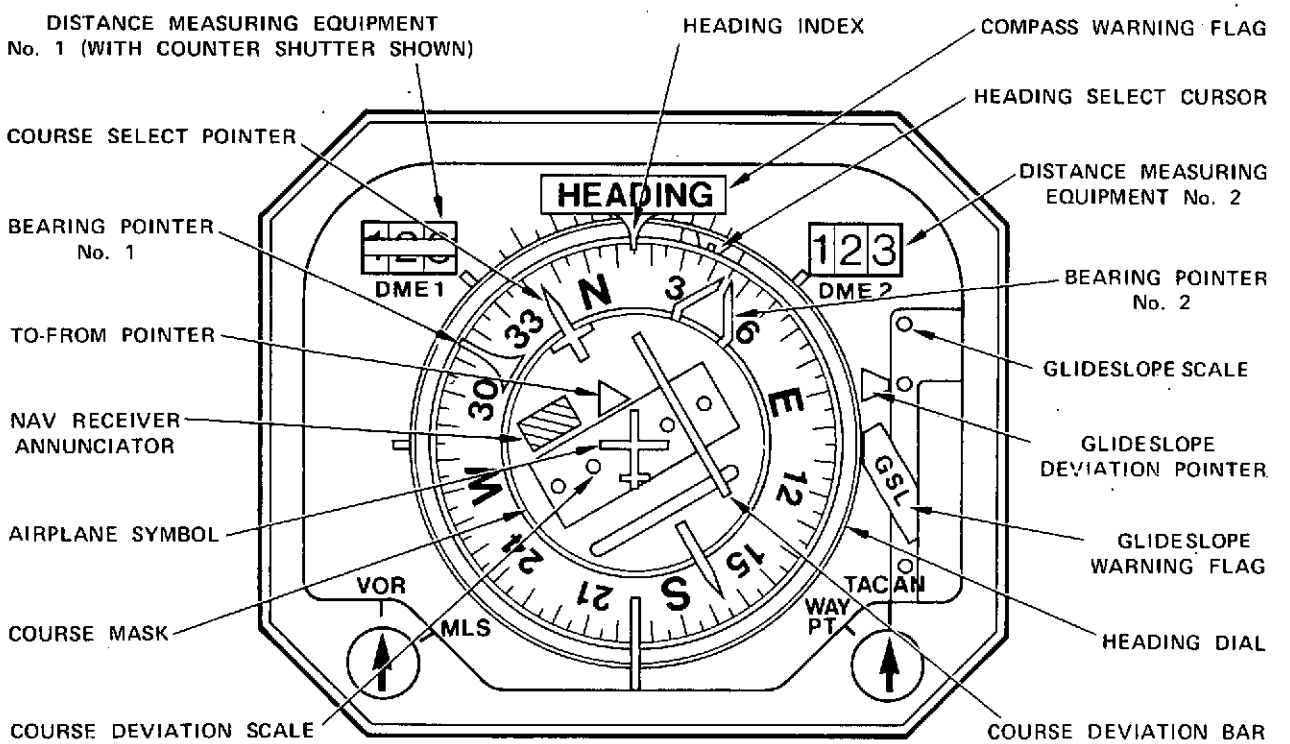

Figure 10.—Horizontal situation indicator.

Multifunction Display (MFD)

The third instrument displaying navigation data is the multifunction display unit. It is a CRT instrument shown in figure 11. The horizontal navigation data are presented in the form of a map on which the location of the aircraft is displayed. The display can be selected as NORTH UP, COURSE UP, or HEADING UP. For COURSE UP and HEADING UP displays, the aircraft symbol remains stationary and the map symbols move. The four-dimensional guidance status of the aircraft is displayed in the left lower corner of the MFD. Via keyboard

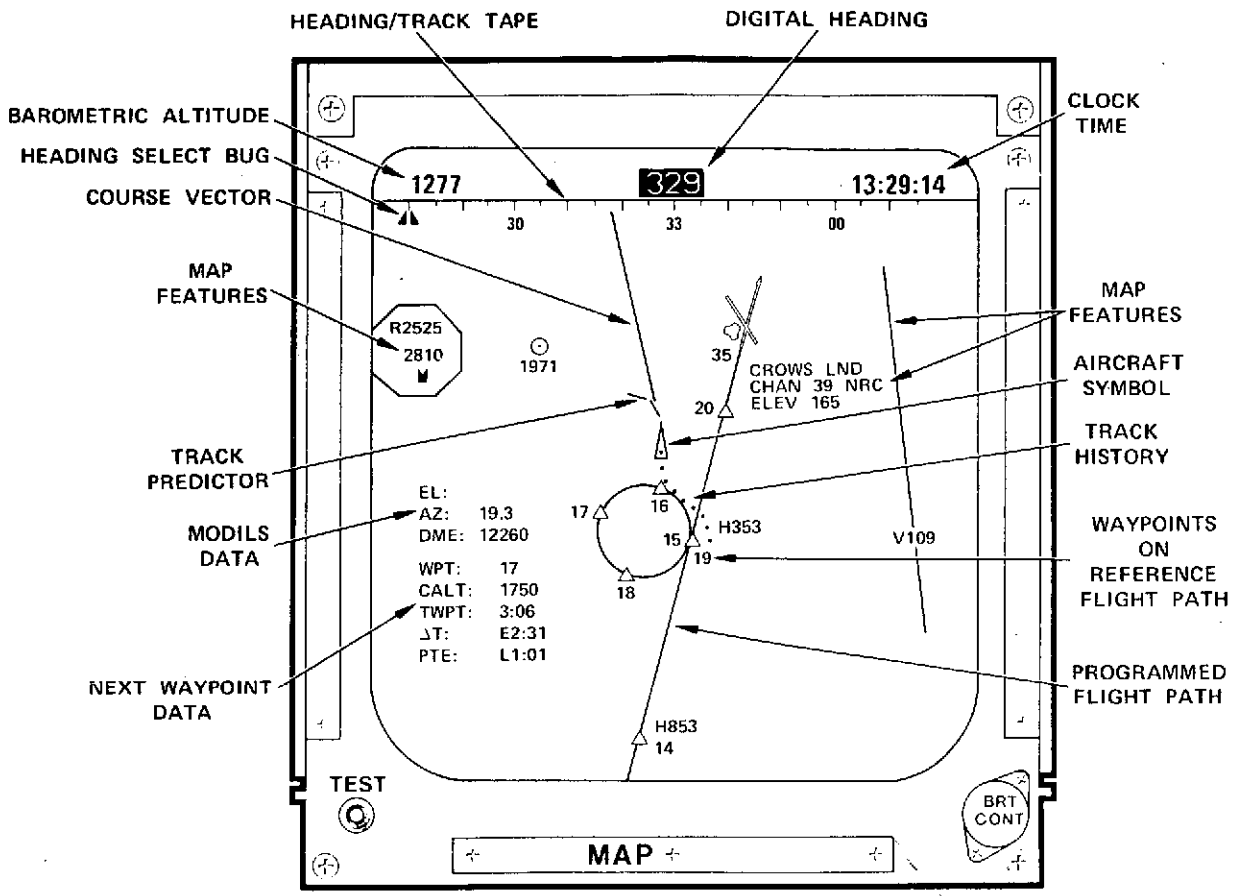

Figure 11.—Multifunction display unit.

selection, the whole angle information of the MODILS (azimuth and elevation) and the MODILS/DME can be displayed as shown. Absence of numerical data on the MODILS display indicates that the signal is not valid (e.g., the lack of elevation data in the figure indicates the data are invalid).

This description of the navigation data displays completes the description of the navigation system. The next section will be devoted to navigation flight and simulator test results.

SIMULATION RESULTS

The simulation has been designed to validate the flight software and hardware. All the STOLAND hardware items except for the servos and the servo interlock unit form part of the simulation, and the software for flight and simulation is identical. The keys to the realistic simulation are the airplane, wind, and navaid models in the simulation computer (EAI 8400) and the airborne hardware simulator (AHS). The AHS converts digital sensor simulation signals from the EAI 8400 to the formats of the airborne sensors and navaid receivers.

For simulation, six digital two-way channels are available to transfer data from the airborne computer to the simulation computer. Any results of STOLAND computations can be transferred to the 8400 to be further processed and displayed on a strip-chart recorder. For purposes of studying the simulation results, one must be aware that the navigation system sends position and velocity estimates and alternately the wind estimates to the 8400. The 8400 then computes estimation errors.

For interpretation of the simulation results, one must be aware that the strip-chart recorder outputs of the errors contains errors that are due to the comparison of present position data in the simulation computer with navigation data from the airborne computer, which is about 0.1 sec old. In the time interval the airplane flies $\Delta X = 0.1\dot{X}$, $\Delta Y = 0.1\dot{Y}$. For example, this results in a ±7.32 m simulation error when the aircraft flies at 140 knots along a particular coordinate axis. Quantization errors have different patterns as a function of the direction of flight. Figure 12 shows the input errors $\hat{X}_e = X_R - X$ and

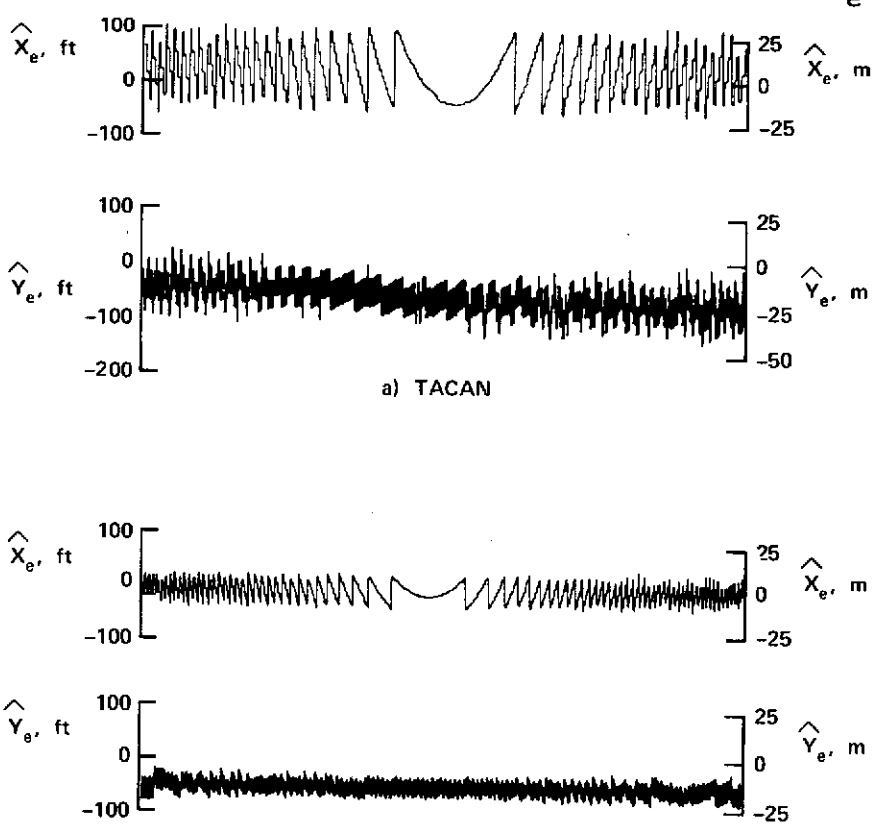

Figure 12.—Flight across centerline of the runway
X = constant TACAN and MODILS raw data.

$\hat{Y}_e = Y_R - Y$ to the complementary filters after the quantized data, azimuth, and DME, are properly coordinate-transformed. In figure 12, the fast changing quantity is azimuth. Both MODILS and TACAN show similar error patterns except that MODILS errors are smaller since MODILS data are more finely quantized. The next figures show the effect of quantization when flying along the centerline of the runway.

In figure 13a the Y-error is primarily caused by azimuth quantization; hence, the error reduces with closer approach to the station. The X-error is primarily due to DME quantization, an effect that changes little with distance from the

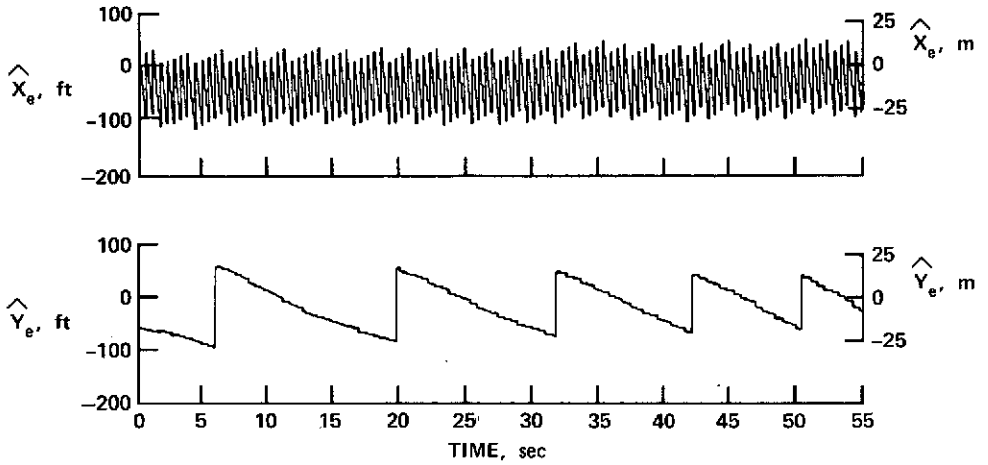

(a) Raw data.

Figure 13.—Position errors due to quantization only on a straight-in TACAN approach.

station. The effect on the filtered estimates is shown in figure 13b. The X-complementary filter removes the high-frequency X-errors but the Y-error shows low-frequency variations. The cause of the apparent bias errors is a simulation error, which has been explained.

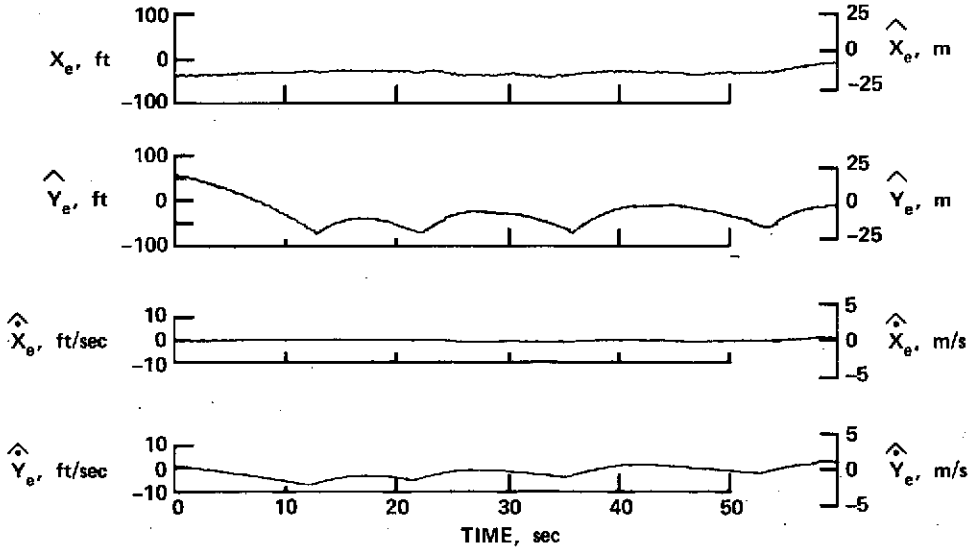

(b) Filtered data.

Figure 13.—Concluded.

Figure 14 shows both raw and filtered TACAN and MODILS errors when flying a circular path in the area of MODILS coverage. For figure 14, no navaid bias errors were simulated. Also, accelerometer errors are not modeled in the simulation. The Y-errors are not shown because they are similar.

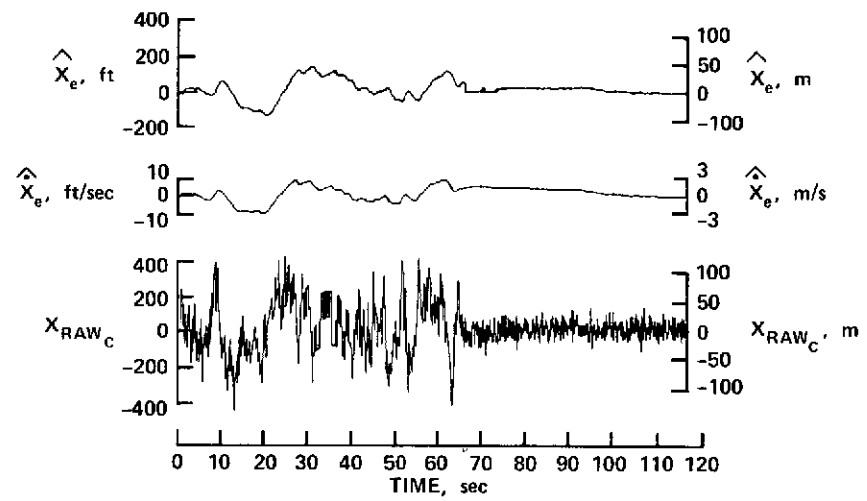

Figure 14.—Comparison of filtered and unfiltered navigation errors.

Comparing figures 13b and 14 it can be seen that the quantization errors are relatively small compared with the random errors. In figure 14, the removal of the high-frequency components of the noise by the filter may be seen by comparing X_R and $\hat{X}_e$. Note, as can be expected from the filter structure, position and velocity errors are highly correlated. Also the MODILS errors are very small. In the TACAN region the standard deviations of the X, Y and $\dot{X}$, $\dot{Y}$ errors are approximately equal and are 24 m and 1.2 m/sec, respectively.

The random errors are small compared to the bias errors of the TACAN system. See appendix I for the error models. The solid lines of figure 15 show the effect of switching from TACAN to MODILS when TACAN has typical errors of az = 1.2° and DME = 305 m. The example is for switching at the beginning of a turn toward the MODILS station. If the switching is done at the end of the turn, the errors will be similar. It will be seen that the position errors from the inaccurate TACAN system to the accurate MODILS are reduced smoothly with a time constant of about 20 sec. However, the velocity errors are quite large and take a long time to settle out (see dashed lines in figure 15). Since it is the goal to turn onto the final straight in glideslope and localizer tracking about 1 min to touchdown, the velocity transients are unacceptable, as will be shown later.

Therefore, as described earlier, at the beginning of navaid switching the acceleration bias error compensating input of the X and Y filters (figure 5b) was removed for 15 sec. Then, the estimate of $\dot{X}$ and $\dot{Y}$ will change only due to accelerometer inputs and the $\hat{\dot{X}}$ and $\hat{\dot{Y}}$ transient responses will be little affected (see solid lines in figure 15).

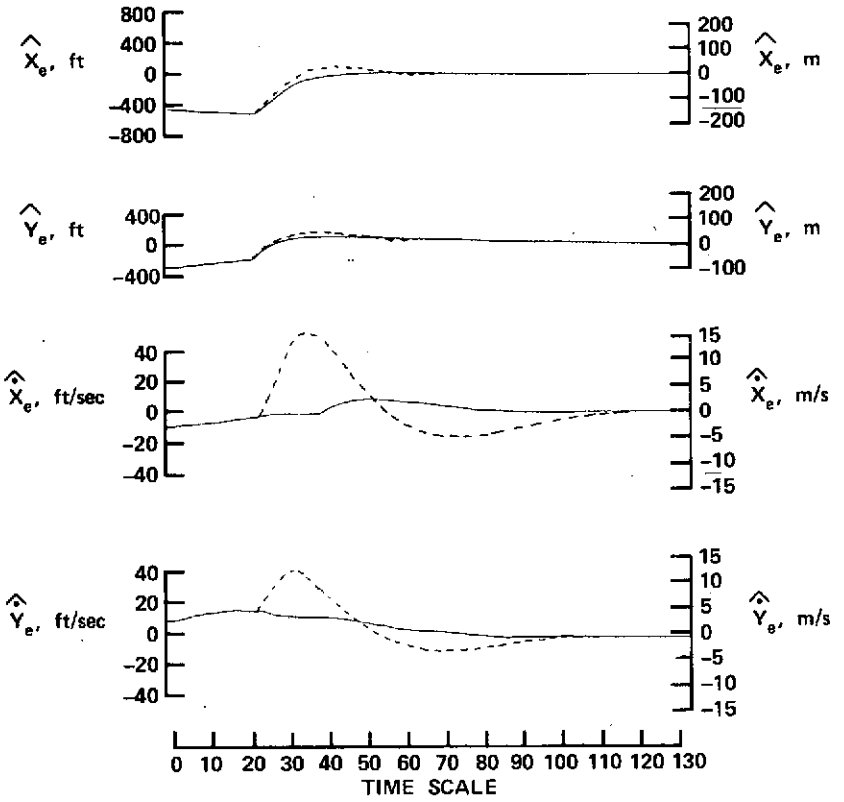

Figure 15.—Navigation errors compared when switching from TACAN to MODILS with the acceleration bias compensation loop opened for 15 sec and closed.

The resulting improvement in path tracking is shown in figure 16, where the flightpath was a descending turn onto the final leg. The path was flown with and without compensation loop switching. With switching, the navigation

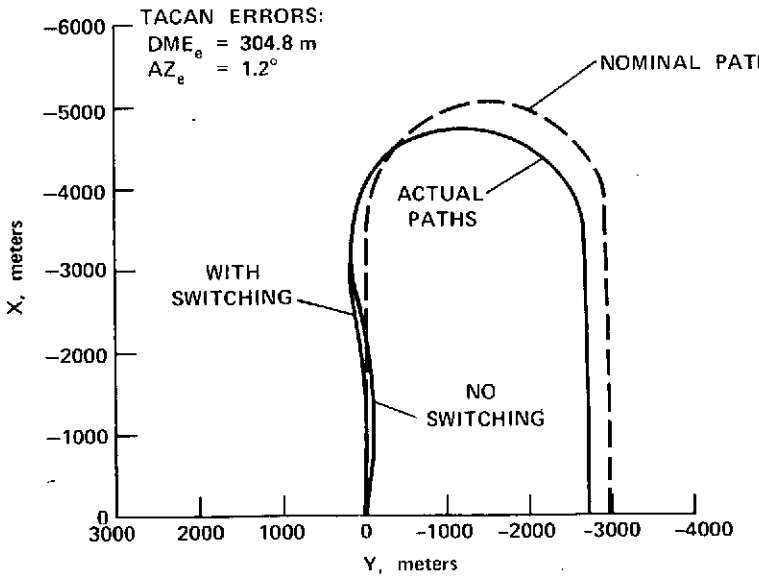

Figure 16.—Flightpaths compared when switching or not switching out the acceleration bias compensation loop.

errors during transition are now smaller, especially the speed estimate errors. Since localizer tracking is based on a roll command $\phi_c = K_1 Y + K_2 \dot{Y}$ the flightpath prescribed by the precision guidance system is more quickly acquired without overshoot.

The magnitude of navigation errors that are introduced due to errors in onboard measurements of the Euler angles, θ, ϕ, and ψ, and the body axis accelerations must be determined. Only the effects of bias errors of representative magnitudes were investigated. During simulated flights of straight and circular flightpaths at constant altitude, errors were introduced into the measurements one at a time with no other navigation errors except quantization errors present.

During level unaccelerated flight or constant ground speed coordinated turns, the outputs of the X_B and Y_B accelerometers will be small. Transformation of these accelerations through the Euler angles to the runway coordinate system will be small, independent of small errors in the acceleration and Euler angle measurements. Thus, navigation errors due to the above will be negligible.

Effects of constant accelerometer bias errors on the navigation errors are small. For the $\dot{X}$ and Y filter the final value theorem applied to $X_R(s)/\ddot{X}_R(s)$ and $\dot{X}_R(s)/\ddot{X}_R(s)$ of equations (21) and (22) shows that the steady-state outputs are zero. The simulation results confirm this. For the Z-filter a nominal bias error of 0.03 g will result in steady-state errors of $\dot{Z}_e = 0.76$ m/sec and a $Z_e = 0.76$ m, which is also small, except for landing. For flight to touchdown it is necessary to switch to radar altimeter data. This has not been implemented in the CV-340 flight program but will be in the Twin Otter and Augmentor Wing programs.

We will now determine the effects of Euler angle measurement errors. The measured accelerations in a coordinated level turn and level flight will be $a_x = g\theta$, $a_z = g/\cos\phi$. Making small angle assumptions for θ and ψ_E, ϕ_E, θ_E, the Euler angle measurement errors, the acceleration errors in the aircraft axis horizontal coordinate system will be from equation 17.

$$\begin{bmatrix} \ddot{X}_{A'_E} \\ \ddot{Y}_{A'_E} \\ \ddot{Z}_{A'_E} \end{bmatrix} = \begin{bmatrix} -g\ \theta_E \\ g\ \phi_E \\ g\ \phi_E \tan\phi \end{bmatrix} \tag{32}$$

As shown previously, the third order X and Y filters will have no steady-state output errors in unaccelerated level flight, and effects of roll measurement errors induced by tight turns will be washed out quickly when the filter gain is sufficiently high. Also there is no steady-state output error in unaccelerated level flight because the $\ddot{Z}_{A'_E}$ is zero for level flight.

In a turn, the error inputs to the X and Y filters are time-varying, and a changing input is applied to each filter while the bank angle changes

$$\begin{bmatrix} \ddot{X}_{R_E} \\ \ddot{Y}_{R_E} \\ \ddot{Z}_{R_E} \end{bmatrix} = \begin{bmatrix} g[(-\theta_E - \tan\phi\ \psi_E)\cos\psi - \phi_E \sin\psi] \\ g[(-\theta_E - \tan\phi\ \psi_E)\sin\psi + \phi_E \cos\psi] \\ g\ \phi_E \tan\phi \end{bmatrix} \tag{33}$$

A continuous turn results in sinusoidal acceleration error inputs to the X and Y filters. As a check on equation (33) and to get a feeling of the error magnitudes involved, a 3° heading bias error was simulated, while flying at a bank angle of 30° and completing a full turn every 85 sec. This gives a turning frequency of $\omega = 0.075$. From equations (20) and (21) the amplitude ratios at that frequency are $\hat{X}/\ddot{X} = 17.05$ and $\hat{X}/\ddot{X} = 79.5$. From equation (33)

$$\ddot{X}_{R_{Emax}} = 32.2 \tan 30° \frac{3°}{57.3} = 0.975$$

which results in $\dot{X}_{Emax} = 5.06$ m/s and $X_{Emax} = 23.6$ m. These values compared to simulator measurements within 5%.

Figure 17 shows the effect of blending barometric and MODILS altitude information on the altitude and vertical speed estimates. The errors were recorded while simulating a landing approach followed by a go-around. For this record, MODILS random noise errors were simulated in the 8400 and the barometric altimeter noise was approximated in the Airborne Hardware Simulator where the digital barometric pressure information from the 8400 was converted into a frequency via a voltage-controlled oscillator. Observing figure 17, the altimeter has a bias

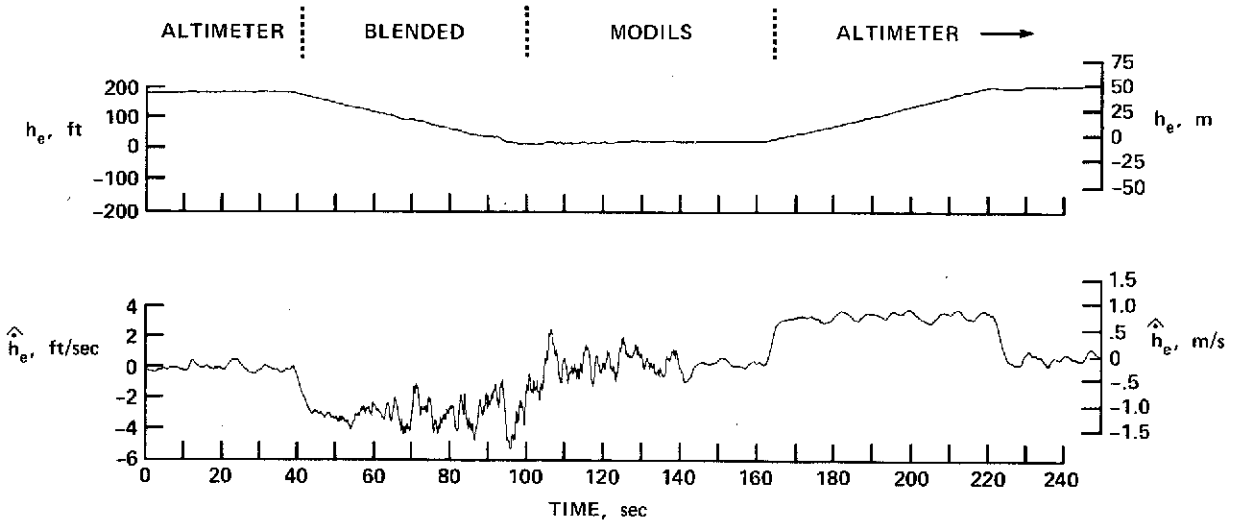

Figure 17.—Altitude and altitude rate estimate errors in different phases of the flight.

error of 55 m. When in MODILS coverage, the blending of barometric and MODILS data continues for 1 min. Since no bias error was simulated for MODILS, the altitude error during MODILS coverage is zero. Upon go-around, MODILS coverage is left but a computed bias correction is applied to the barometric altimeter reading, which prevents a sudden jump of the altitude estimate. This bias error is linearly removed in 1 min. During the transition periods, an average vertical speed measurement error of 55/60 = 0.91 m/sec occurs. Also, the character of the baroaltimeter noise is different from that of the MODILS noise.

FLIGHT TEST RESULTS

For flight tests, a set of data similar to that for the simulator tests is required. Table 1 shows the data list of 50 digital words that are recorded at chosen rates between 1 and 20 times per sec. For specific tests, the data list can simply be changed to put out any data quantity that resides inside the computer.

For navigation tests, an accurate position and speed reference system is required. This is provided by radar tracking with a precision Nike Hercules radar system located as shown in figure 2. The tracking data is time-tagged and recorded on a serial digital PCM tape. For postflight analysis, radar data are smoothed and combined with the airborne data in data sets. Data analysis can be achieved via FORTRAN programs. We shall now examine the flight data.

The results of the tests will be demonstrated by data from a single flightpath. The flightpath, shown in figure 18, is defined by a series of waypoints.

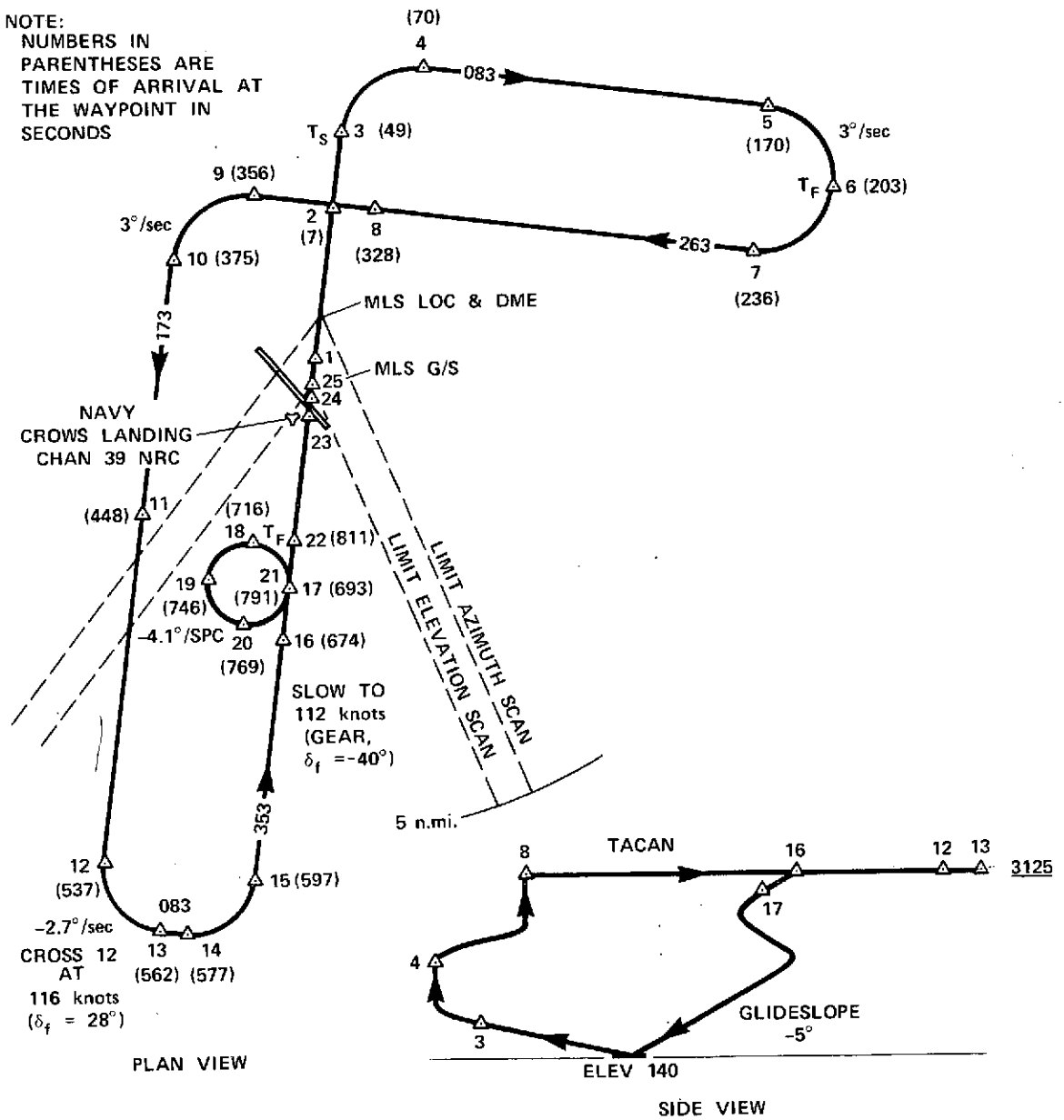

(Numbers in () are times of arrival at the waypoint in sec.)

Figure 18.—Reference flightpath.

TABLE I.—STOLAND Data List

Word No.	Parameter Description (Mnemonic)	Word No.	Parameter Description (Mnemonic)
1	Time Code (TCG1)	21	Pitch CWS Command (ZC8)
2	Time Code (TCG)	22	ACCYB (flight) XTRUE (sim)
3	Glide Slope Deviation (flight) (G/SDEV) ZDOTTRUE (sim)	23	X Coordinate [ZN(2)]
4	Localizer Deviation (flight) (LOCDEV) YDOTTRUE (sim)	24	Y Coordinate [ZN(4)]
5	Pitch FD Command (DELPFD)	25	X Navaid (XRN)
6	Roll FD Command (DELRFD)	26	Y Navaid (YRN)
7	X Wind Velocity (ZC16)	27	4D Error (GDELTS)
8	Y Wind Velocity (ZC15)	28	Y Error (YERR)
9	Z Body Acceleration (ACCZB) (flight) ZTRUE (sim)	29	Time to Go (GTIMGO) (flight) YTRUE (sim)
10	True Airspeed (VTAIRF)	30	SBLGS Range (RSSBRA)
11	Throttle Rate Command (OUTB2+4)	31	TACAN Range (TACRNG)
12	VOR Bearing (PSIVOR)	32	Radio Altitude (RALTF)
13	Aircraft Heading (PSIA)	33	Baro Altitude (BALT)
14	TACAN Bearing (TACBER)	34	Z Coordinate [ZN(6)]
15	Pitch Attitude (THETA)	35	Unfiltered Z Estimate (ZRN)
16	Pitch Command (THTCOM)	36	Z Error (HREFER)
17	Roll Attitude (PHI)	37	X Velocity [ZN(1)]
18	Roll Command (PHICOM)	38	Y Velocity [ZN(3)]
19	SBLGS Elevation (EPSCEA)	39	Z Velocity [ZN(5)]
20	SBLGS Azimuth (PSICA)		

TABLE I.- STOLAND Data List, Concluded.

(Digital Data Bit Position)

Word No.	15	14	13	12	11	10	9	8	7	6	5	4	3	2	1	0
40	Roll RG Valid	Pitch Servo Select	Roll Servo Select	Yaw Servo Select	Latch Throttle Valid	Latch Flap Valid	Radio Alt Valid	A/T Select	SAS Select	Auto Select	Latch Pitch Valid	Latch Roll Valid	Pitch RG Valid	Elevator Trim Select	DME Flag	Vertical Gyro Valid
41	Nozzle Servo Select	Spare	SB G/S Valid	SB LOC Valid	Control Wheel Go-Around	DME in Test	Yaw RG Valid	LOC Mode	G/S Super	VOR/LOC Super	Brg 2 Valid	Brg 1 Valid	TACAN Range Invalid	TACAN Brg Invalid	Throttle Servo Select	Flap Servo Select
42	Throttle Not Min	MSP Valid	WOW	Equip SP Valid	Cockpit SP Valid	MFD DU Valid	MFD SG Valid	EADI DU Valid	EADI SG Valid	PPS Valid	Latch Nozzle Valid	Hdg Select Valid	Course Valid	Hdg Valid	Compass Valid	Latch Yaw Valid
43	Waypoint Number					MFD North Up	MFD HDG Up	MFD Crse Up	Spare	MFD 5 mile	MFD 1.5 Mile	MFD 0.5 Mile	MFD FP4	MFD FP3	MFD FP2	MFD FP1
44	ATS Engage				Nav Director				Roll FD Mode				Pitch FD Mode			
45	Roll Arm				Roll Engage				Pitch Arm				Pitch Engage			
46	Alt Select Arm	Acc Test B	Acc Test A	Trim Inhibit	Flap Valid	Throttle Valid	G/A Com	G/A Rdy	Flare Com	Flare Arm	DH	G/S Capt	G/S Arm	LOC Capt	LOC Arm	G/S Valid
47	Standby	CDI Flag	Display To/From	Yaw RG Test	Roll RG Test	Pitch RG Test	DELECS - Elevator Command									
48	G/S Man	Keyboard	DME 2	DME 1	VDI Flag	To-From	DELACS - Aileron Command									
49	Full Auto	Ref FD	FPA Valid	FD Valid	LOC Valid	Speed Valid	DELRCS - Rudder Command									
50	Hor Nav	Nav Valid	Monitor Test	Pitch Monitor Test	PPS Reset	DME Select	DELFCS - Flap Command									
51	FD	Mag Tape	Spare	Pitch Valid	Roll Valid	Yaw Valid	DELTSO - Throttle Command									

A waypoint is required whenever there is a change in the flightpath caused by a turning or an increase or decrease in either flightpath angle or nominal airspeed. From takeoff to touchdown the experimental flightpath is defined by 24 waypoints. Waypoints 1 to 10 define the climbout profile. The turns in this portion of the flightpath were made to avoid populated areas. Waypoints 10 to 23 define the approach portion of the flightpath. The constant glideslope angle descending turn (waypoints 17 to 21) is a test of the system capability rather than a proposed practical approach maneuver. The landing portion of the flight path (waypoints 23 to 25) was not used in flight, and go-around maneuvers were performed.

During the flight, ground based navigation data are received from TACAN and MODILS, which are positioned as shown in figure 2. TACAN data are received during the complete flight, while MODILS data are received during the approach only. From TACAN error data, given in figure 19, one observes several types of errors which are discussed in the literature. There are bias errors, high-frequency noise, and a low-frequency component of noise. In addition, error spikes which do not fit a Gaussian error model are seen. The length of occurence

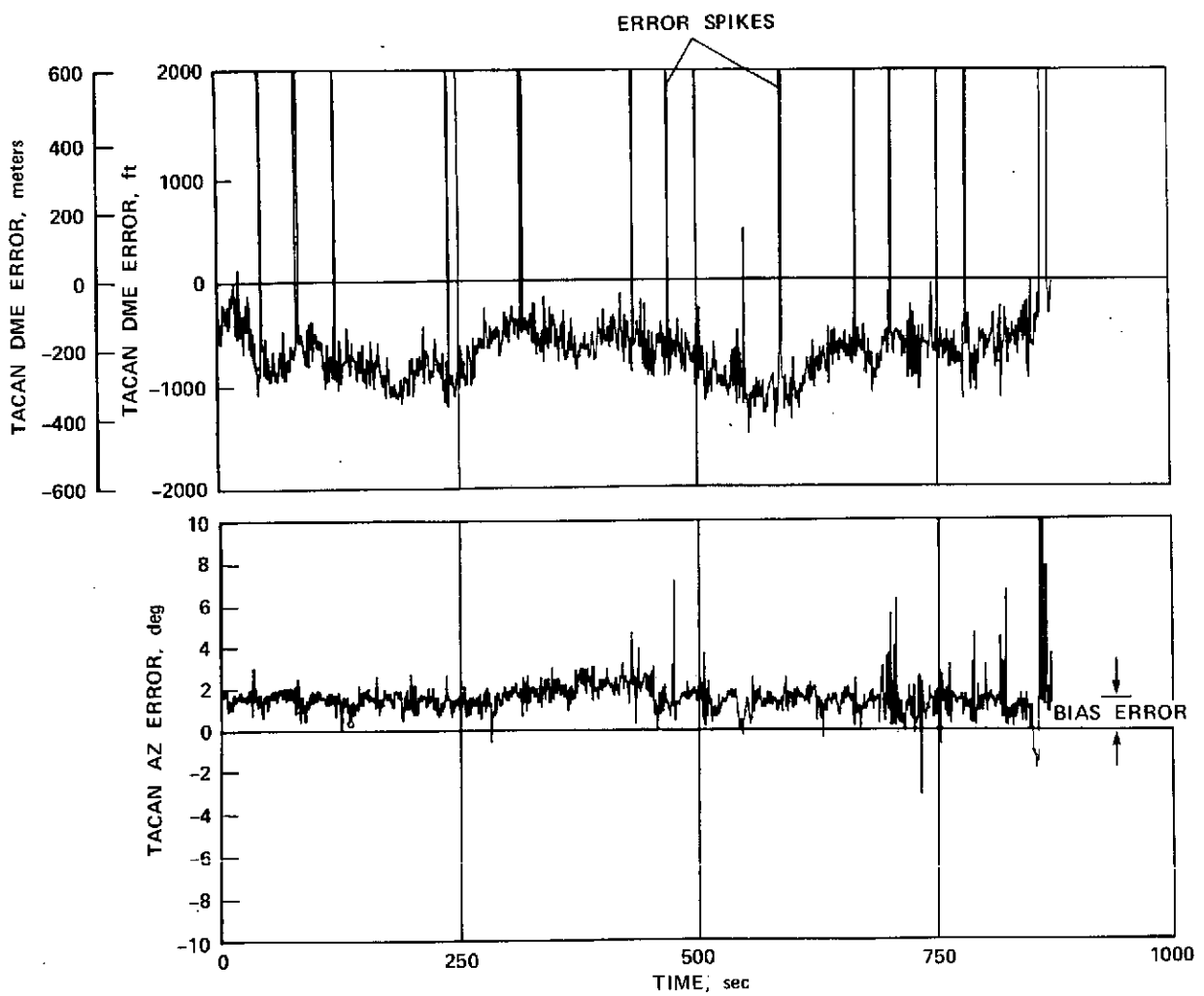

Figure 19.—TACAN error from comparison with radar data.

of these DME errors ranges from 0.5 to 2-1/2 sec. The DME valid signal remains valid when these error spikes occur, causing navigation problems. The exact cause for these errors is as yet unexplained. However, it is clear that the error spikes originate between the ground navigation aid and the airborne receiver and not in the transmission link between the receiver and the computer, since this type of error does not occur in the airborne equipment which is also used in the simulation. Also, on other data transmission lines between airborne sensors and the computer, no such errors occur. The MODILS DME errors and valids shown in figure 20 are similar in nature but considerably smaller.

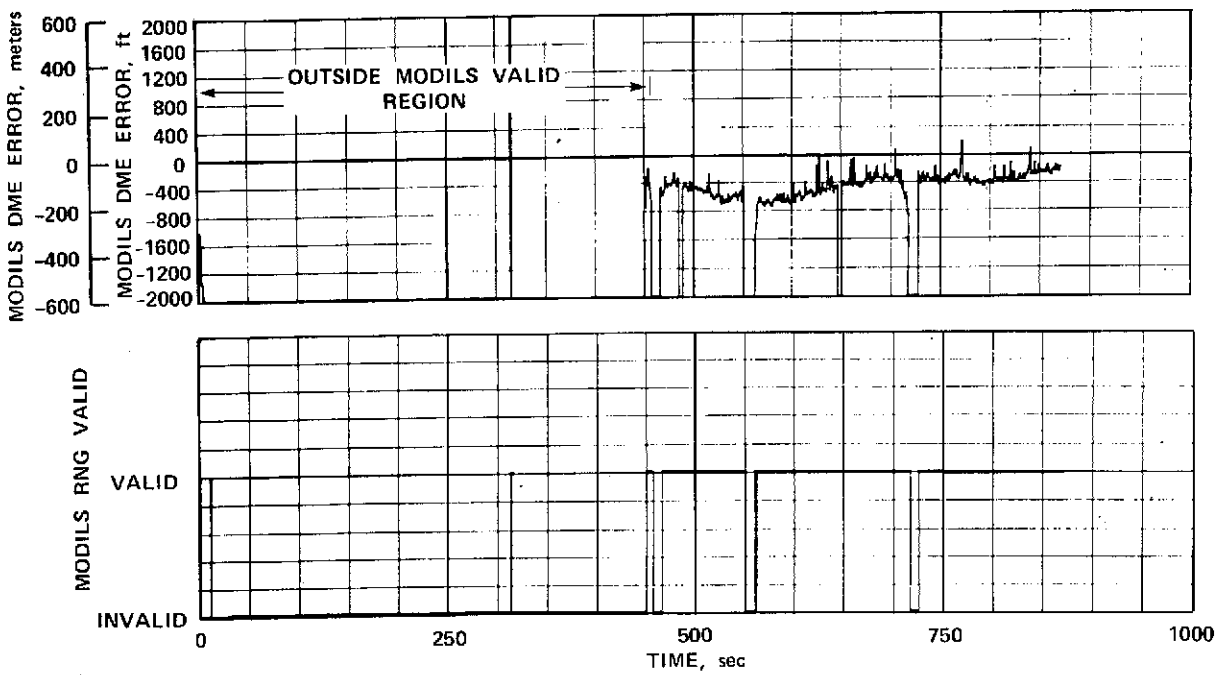

(a) DME.

Figure 20.—MODILS errors and valids.

The large MODILS DME errors are caused by signal dropouts where the receiver synchronization is lost. The DME signals will then read zero. However, for short dropouts, the DME valid flag may not disappear. For longer dropouts, the DME valid reappears for about 1 sec before the DME again gives correct values. These MODILS and TACAN DME dropouts and error spikes are the primary reasons for large input transients to the navigation filters.

The MODILS azimuth valid and elevation valid signals (figures 20b and c) go valid, outside the proportional range of the signal, which necessitated the previously described logic in the software which resets the signal to invalid outside the region of proportionality.

To explain the errors, the MODILS elevation signal is shown in figure 21. The considerable changes of elevation angle, especially the peak at 720 sec, are explained by the descending spiral of the flightpath. Note that the low-frequency error component for elevation becomes small when the aircraft is receiving the 5° elevation signal, which occurs between 550 and 600 sec and after 780 sec (see figure 21). This is the angle of the elevation tilt for

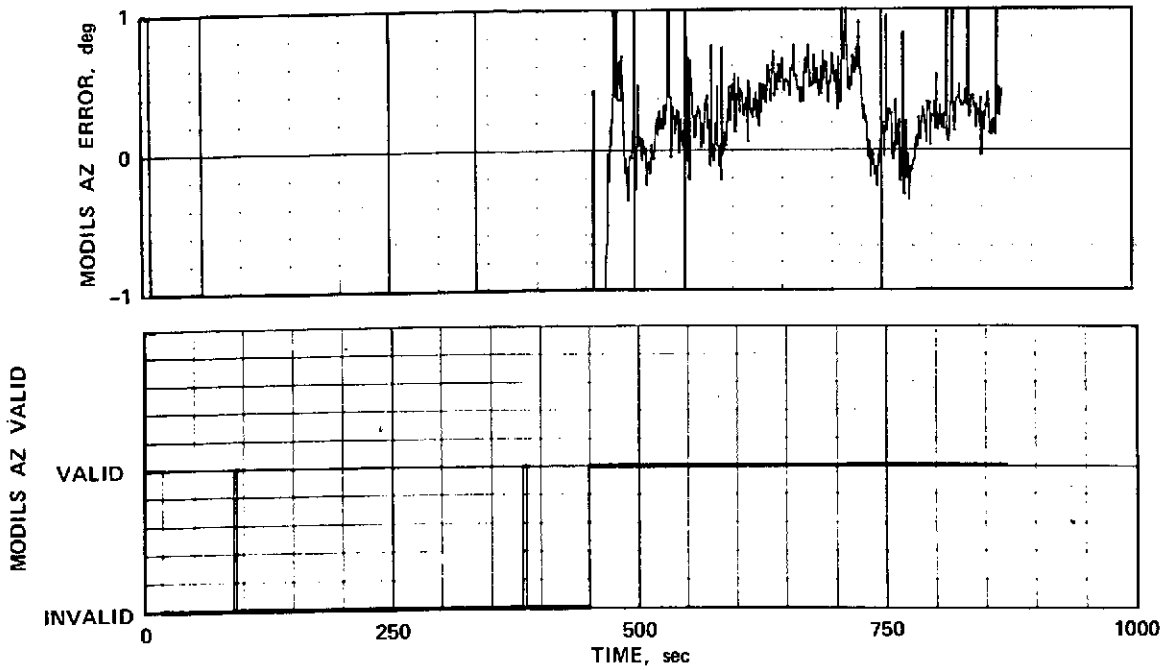

(b) Azimuth.

Figure 20.—Continued.

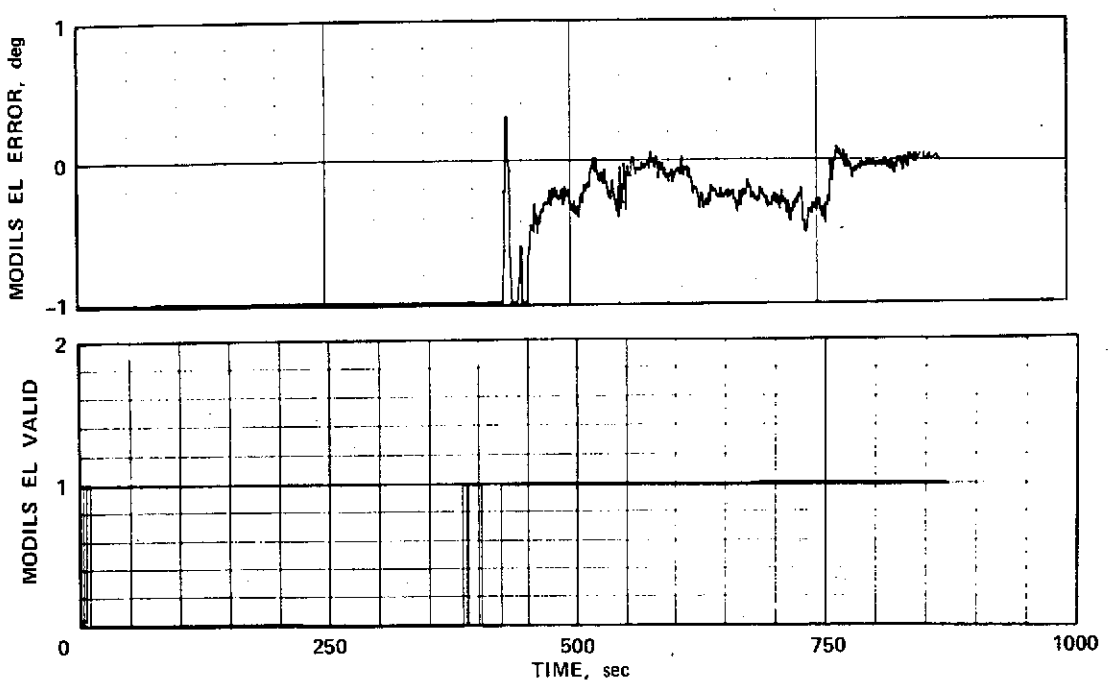

(c) Elevation.

Figure 20.—Concluded.

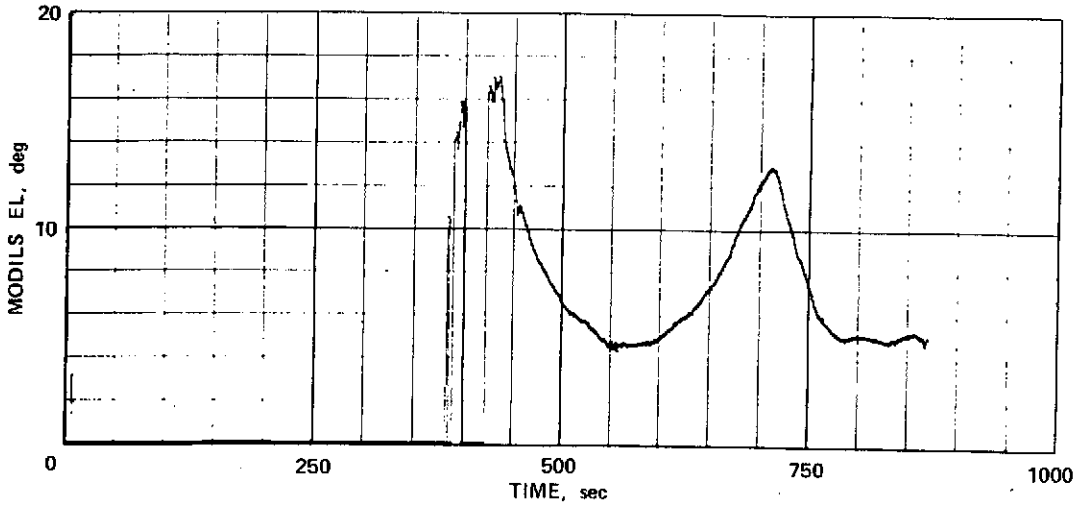

Figure 21.—MODILS elevation.

which the system is calibrated. To give an overview of the range and nature of the input signals to the navigation filters, the signals not discussed as yet are shown in the next three figures.

Figure 22 completes the presentation of the navaid signals.

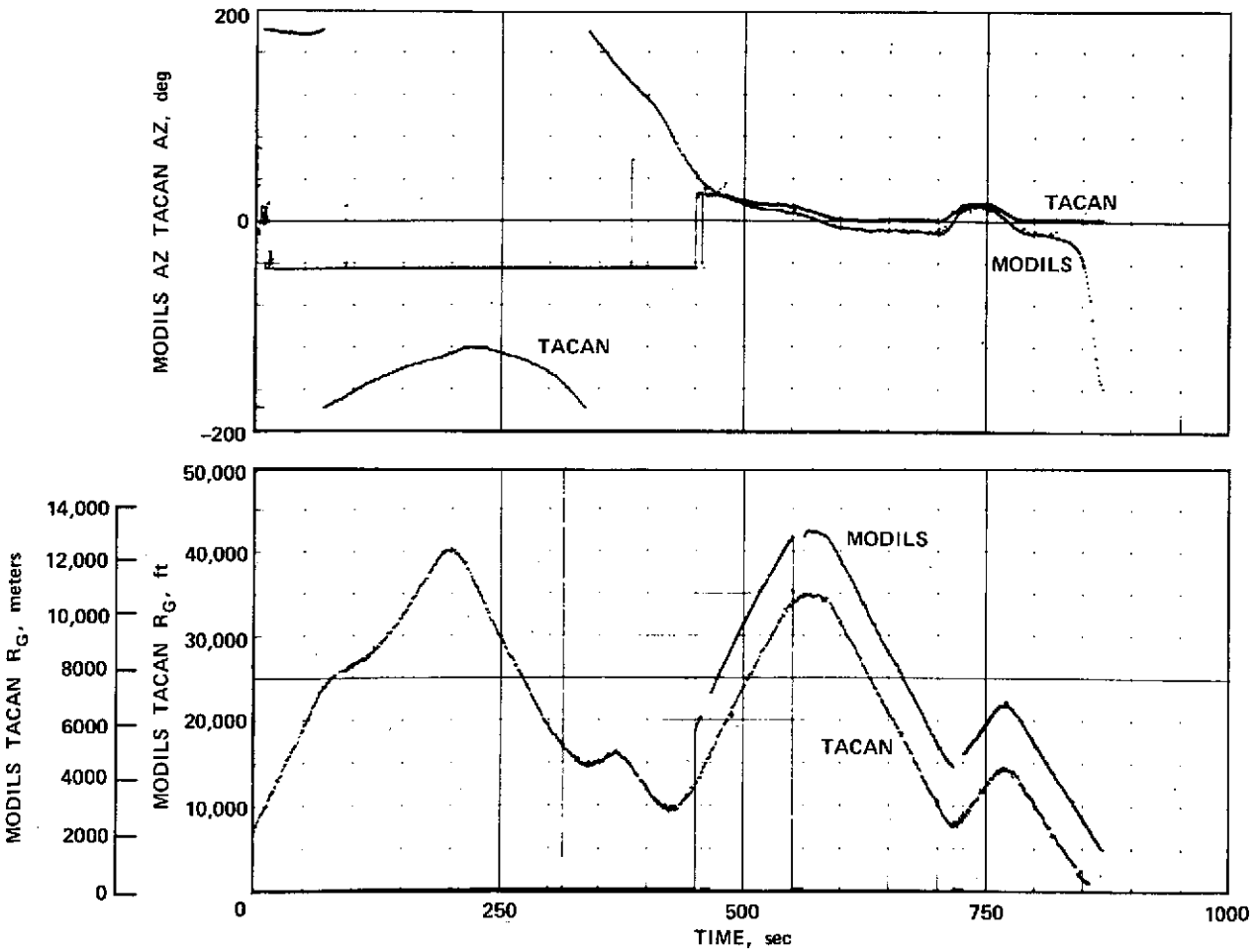

Figure 22.—Navaid signals.

The second set of inputs to the navigation filters are from the body-mounted accelerometers (figure 23) which are translated to the runway axis system via the Euler angles (figure 24).

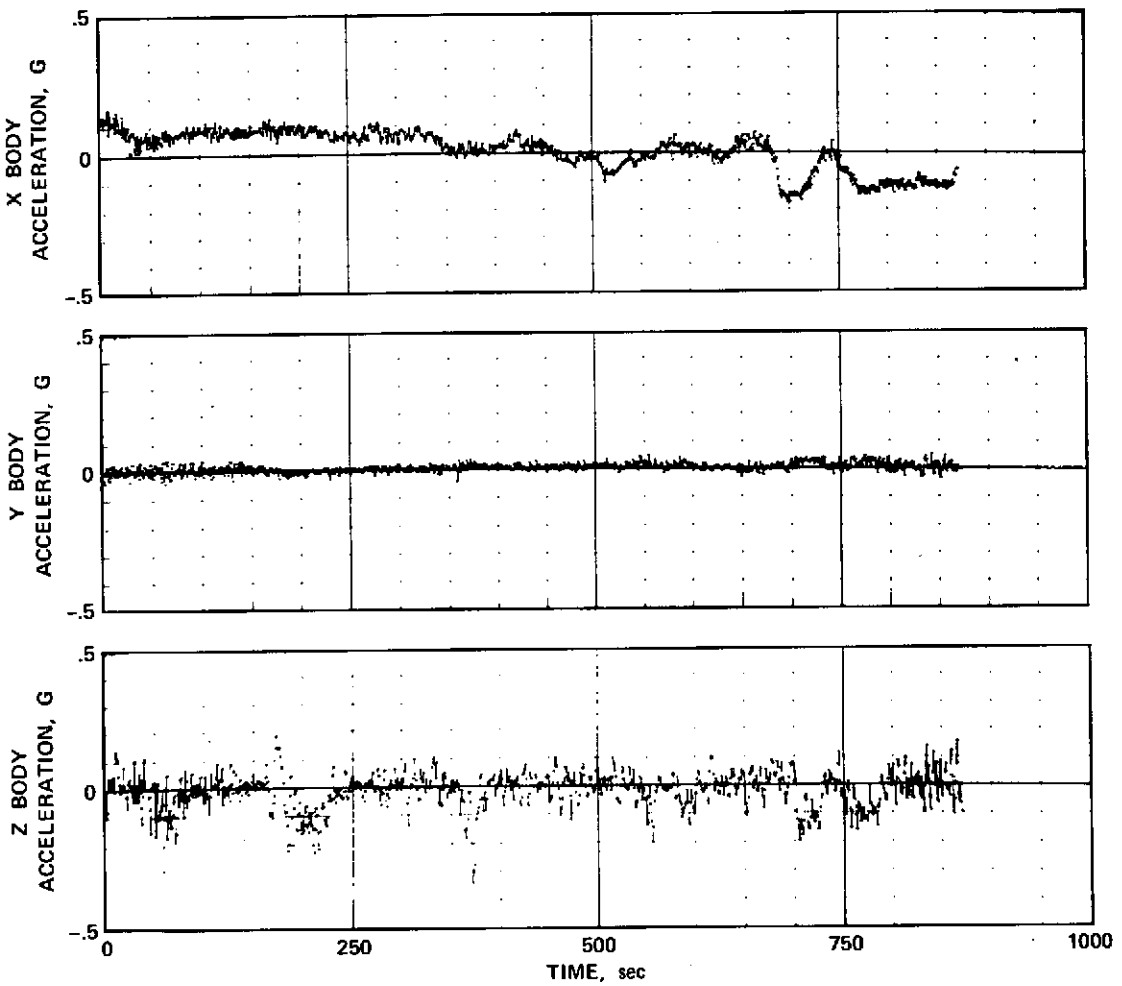

Figure 23.—Body-mounted accelerometer signals.

Figure 25 shows the differences of raw position calculation from the navaid minus the filtered estimate of the same quantity. This results in a good estimate of the high-frequency nature of the input noise to the navigation filters. Again, large spikes due to DME errors can be seen (figures 25 a and b). In addition, transients due to the three TACAN and MODILS transitions can be observed. Since the errors are centered around zero, we see that no bias errors are introduced by the filters themselves. Also, the MODILS high-frequency errors are much smaller than those for TACAN. For most of the flightpath, the barometric altimeter is used as the altitude reference (figure 25c). The high-frequency altimeter noise is extremely small. However, the MODILS elevation introduces peak-to-peak high-frequency errors of up to 30.5 m. As mentioned before, it is necessary to go to MODILS altitude reference towards the end of the 4D flightpath in order to get a smooth transition to glideslope tracking.

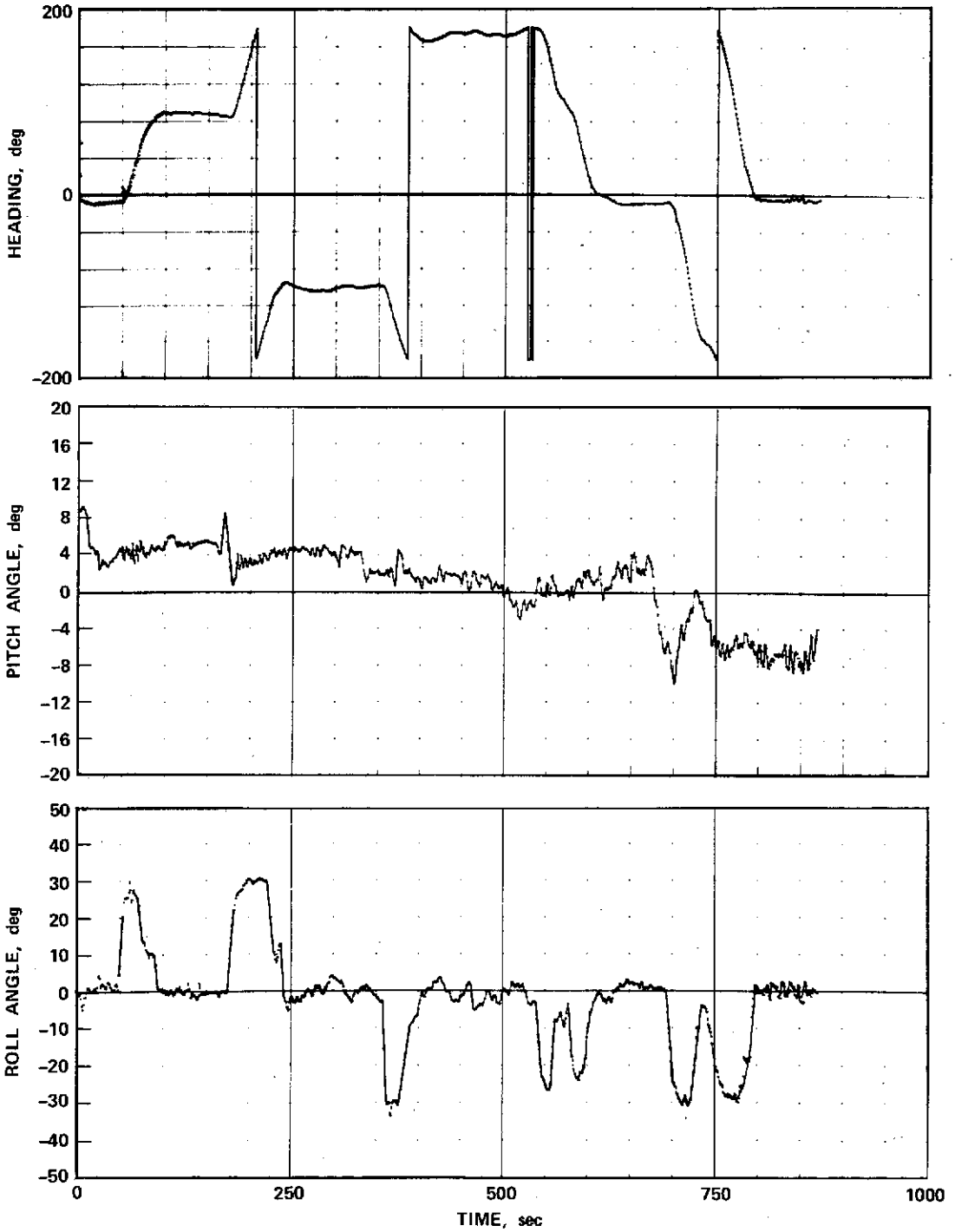

Figure 24.—Euler angles.

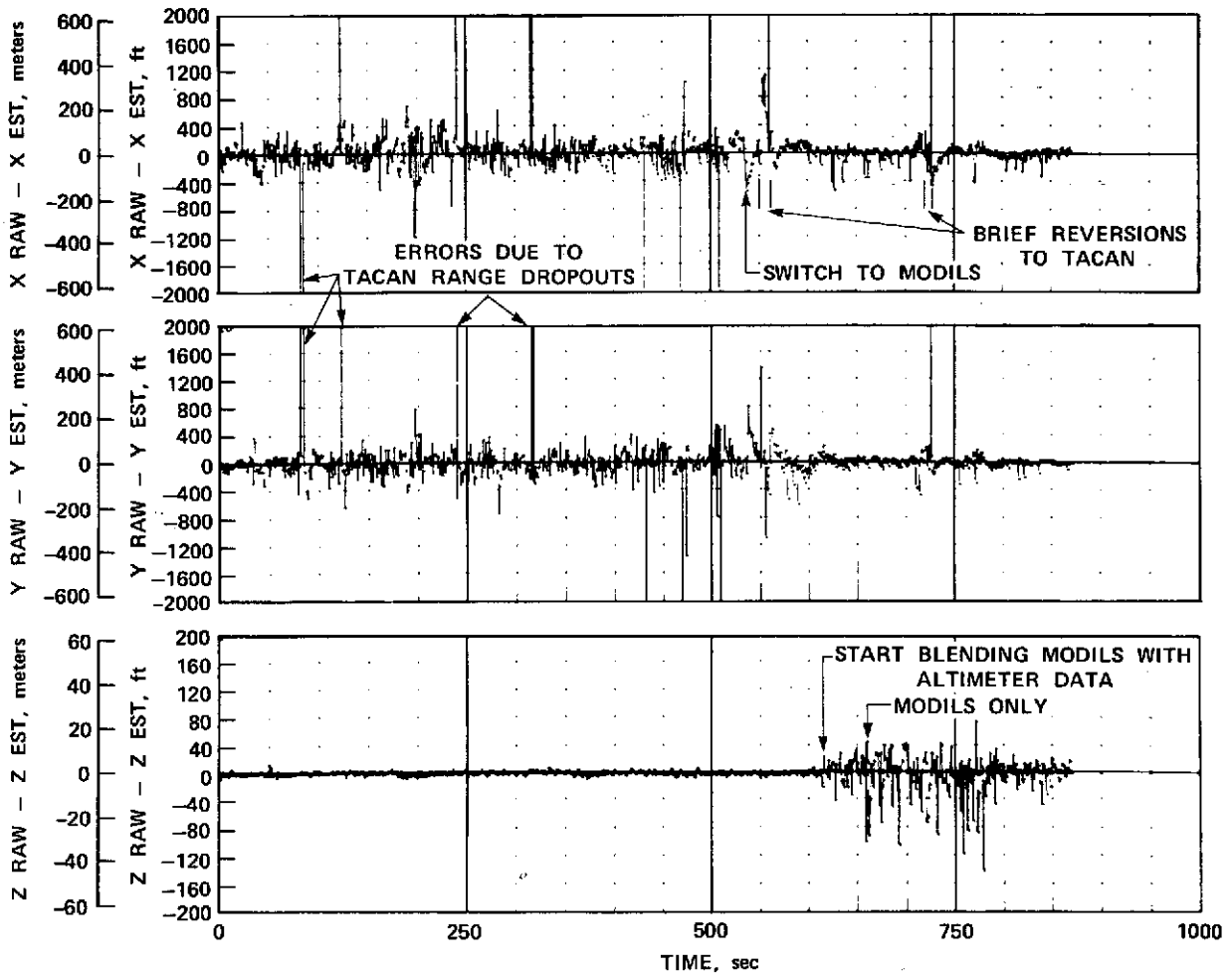

Figure 25.—Estimate of high-frequency position noise input to the navigation filters.

We shall now observe the navigation outputs and compare them with the smoothed radar data. Figure 26 shows the horizontal projection of the approach portion of the flightpath. The switch to MODILS occurred as shown in figure 26, which was designated as the earliest time that automatic navaid switching was permitted. Comparison of the navigation data with radar data shows that the onboard navigation system provides a path estimate that is almost as smooth as that of the offline smoothed radar data. However, the system has no provision to remove the bias errors introduced by the ground based navigation aids. Two reversions to TACAN when MODILS DME dropouts occurred are indicated on figure 26, one in the initial turn toward the final leg, the other during the descending spiral. They caused only negligible transients in the position estimates.

Figure 27 gives a time plot of the estimated ground speed components compared with radar data. The solid line is the navigation estimate and the dotted line the radar estimate.

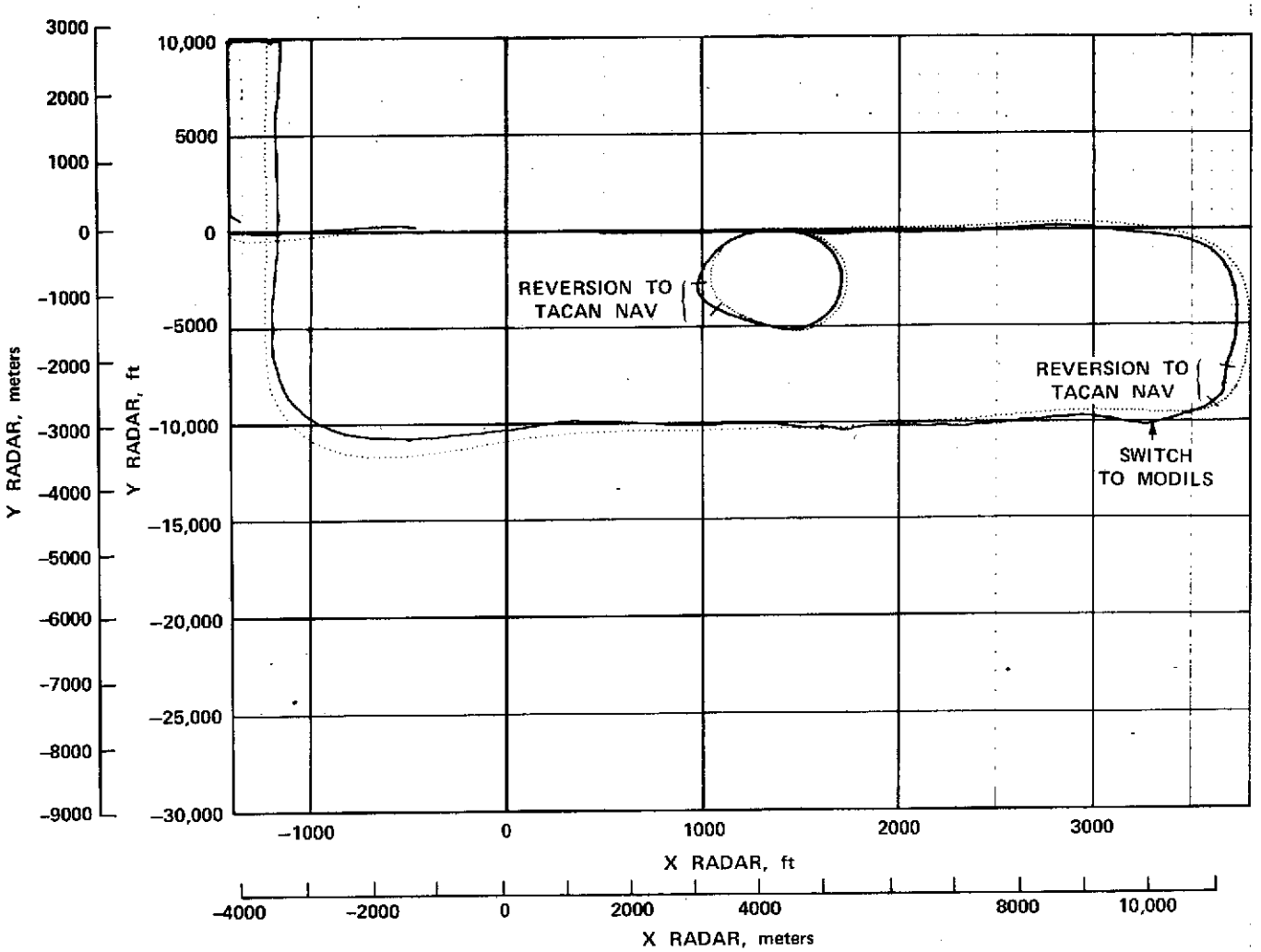

Figure 26.—STOLAND and radar horizontal position estimates.

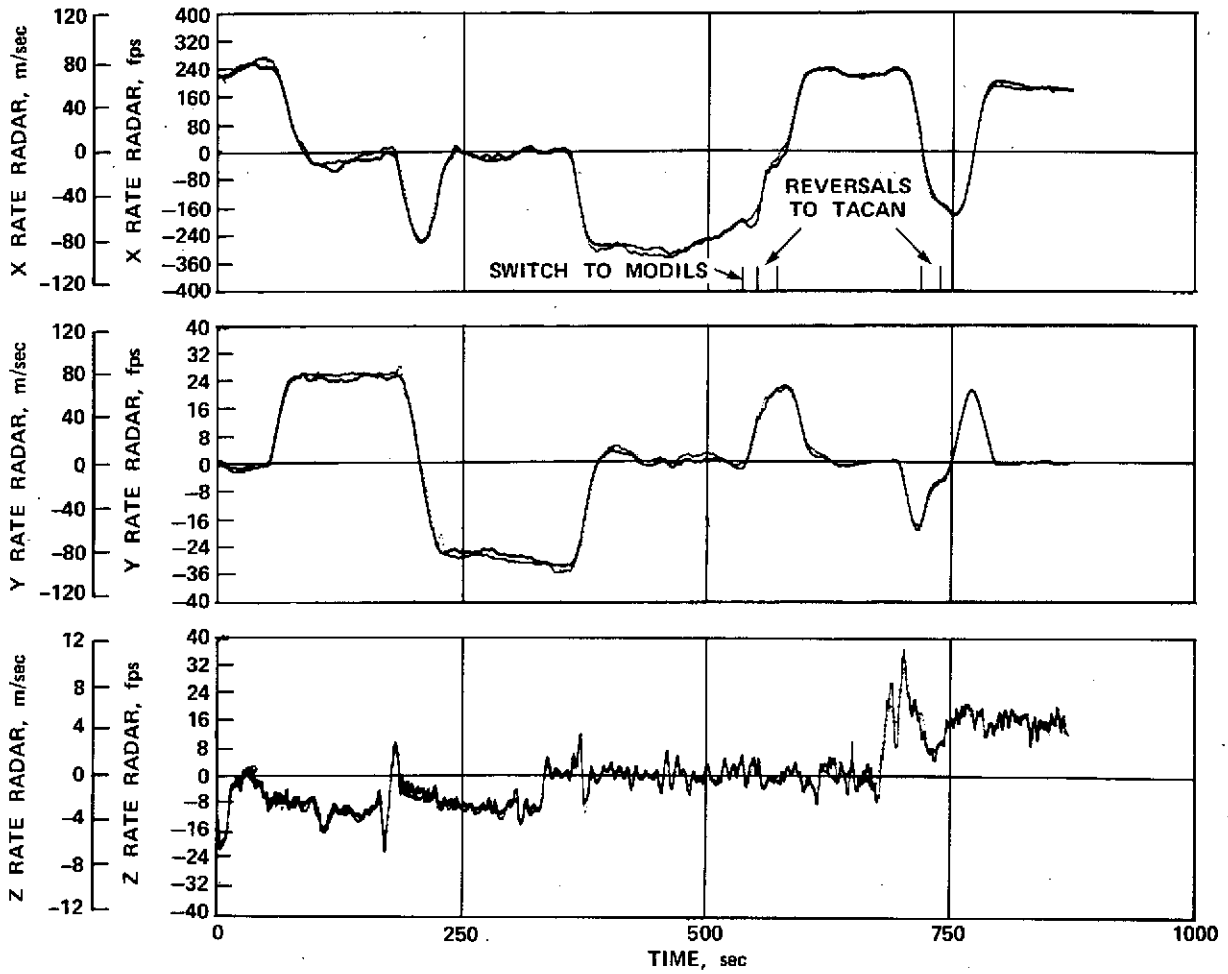

Figure 27.—STOLAND and radar speed estimates.

These filter outputs are needed for the windspeed and groundspeed estimates shown in figure 28, which are important for 4D guidance. The groundspeed estimate of figure 28b has transients at the TACAN to MODILS switch (t = 540 sec) and at the two reversions to TACAN (t = 550 to 570 sec, and t = 720 to 735 sec). Due to the 100-sec filter time constant for the wind estimate, the corresponding wind estimate transients are rather small.

For the flightpath of figure 18, figure 29 shows altitude versus time and figure 30 altitude versus position. Assuming that the wind is relatively constant at constant altitude, and decreases with decreasing altitude, comparison of the wind profile in figure 28 with the altitude profile of figure 29 shows the delay introduced by the wind filters, since the winds reach a plateau around 450 sec (figure 28), while the cruise altitude is reached already at 330 sec (figure 29). Close to ground level, the altimeter error is small since the altimeter is set to the correct present barometric pressure of the airport. During climb to the nominal altitude of 762 m, the altimeter bias error increases

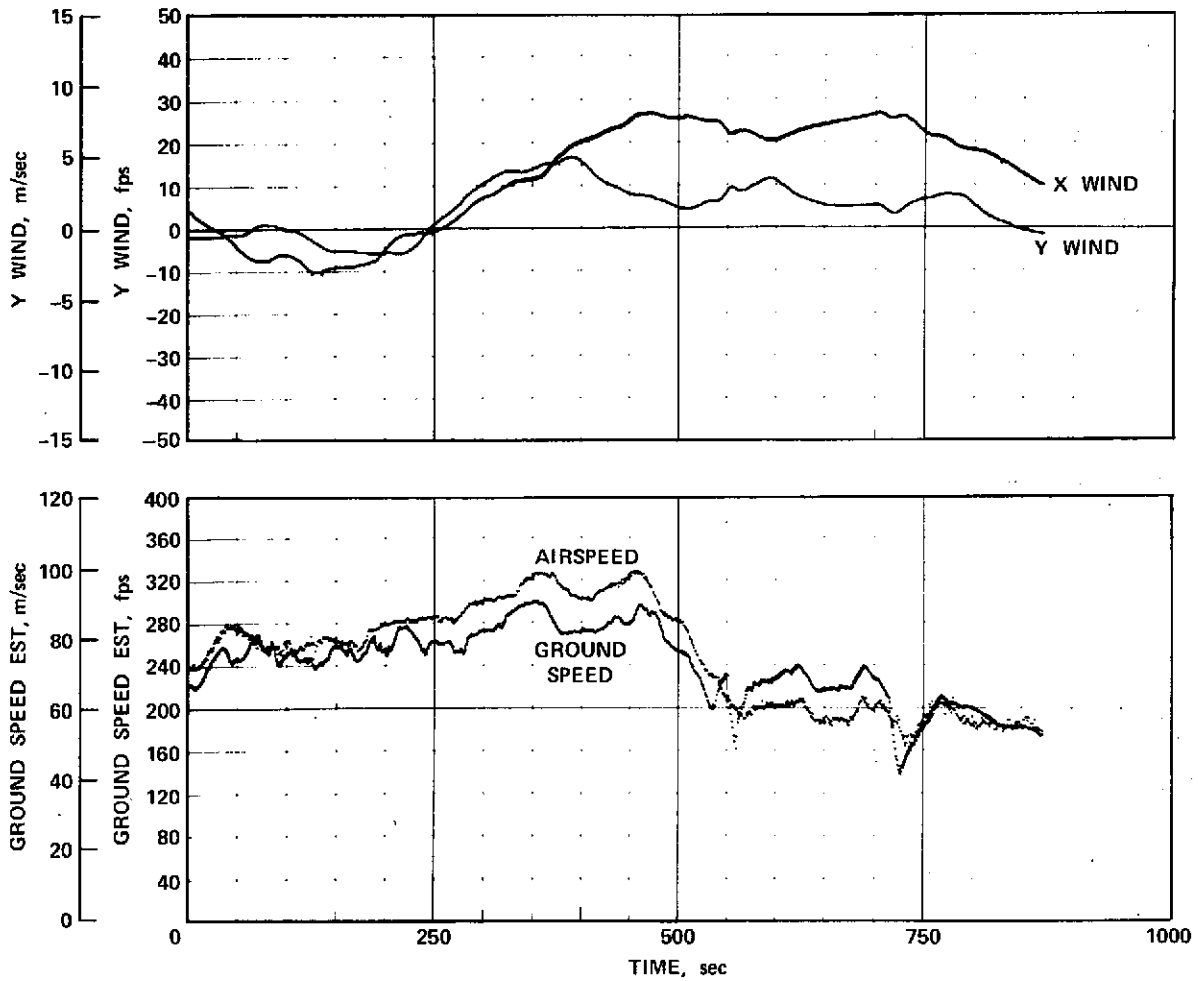

Figure 28.—STOLAND wind- and groundspeed estimates.

to about 46 m, probably due to the effects of the nonstandard atmosphere. At cruising altitude, the estimate is fairly constant but the radar trace indicates that during and after barometric altimeter and MODILS altitude blending the aircraft was actually climbing at an average rate of 0.16 m/s.

Upon descent, the errors again get smaller, as will be discussed later. In figures 29 and 30, the time interval of reversion to altimeter data is also indicated. It can be seen that it does not cause transients in the altitude estimate, thanks to special logic in the altitude blending subroutine.

Finally, we shall look at the navigation errors for this flight (figures 31 and 32). During navigation using TACAN, the large scale errors in X and Y vary almost linearly as indicated by dotted lines. The coarse structure of these errors is explained by the variation of azimuth bias $\Delta\psi$ as well as DME bias and scale error $\Delta R = R_{bias} + K_s R$ which result in the corresponding position estimate errors:

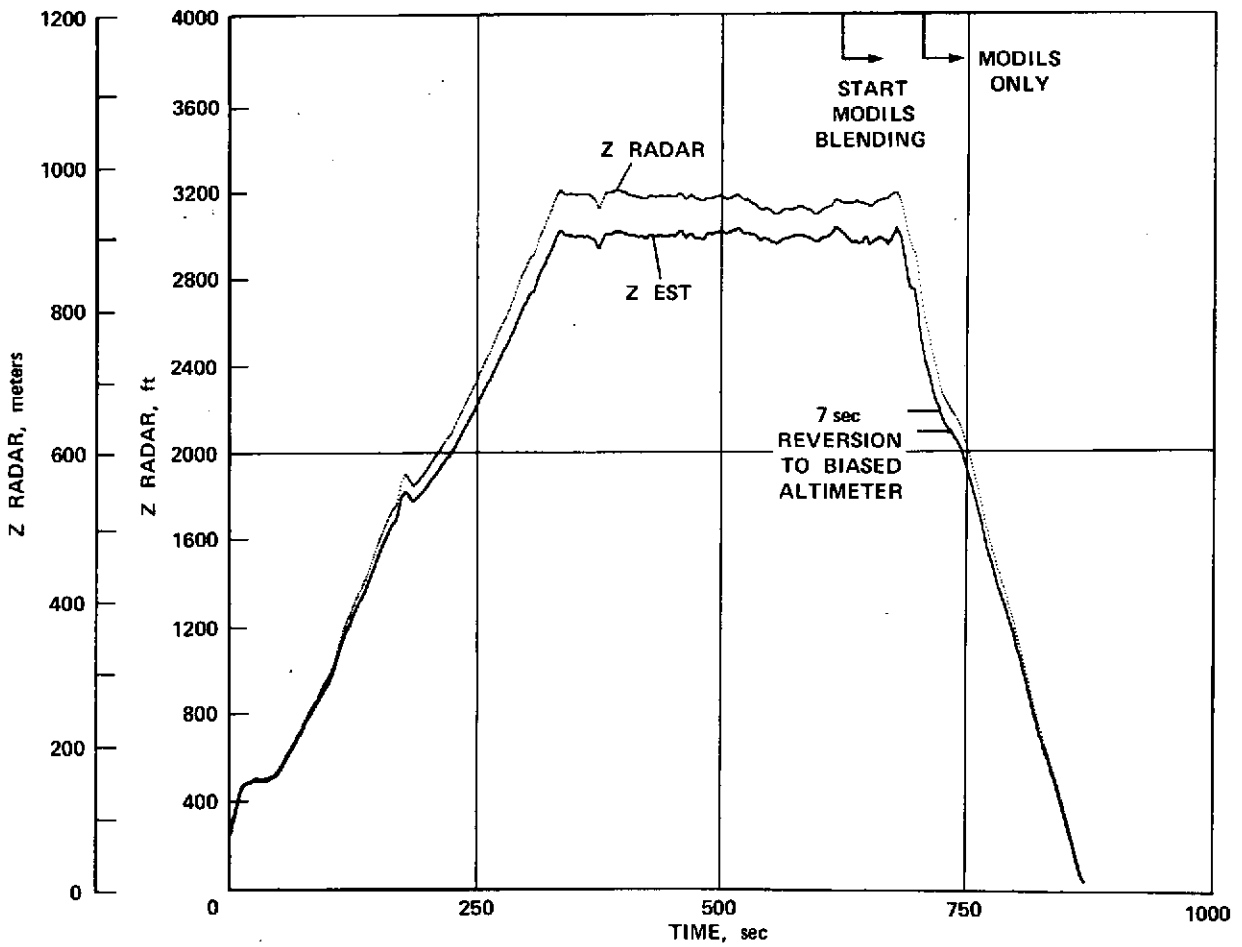

Figure 29.—Time history of vertical flight path profile.

$$\hat{X}_e = \Delta R \cos \psi - R\Delta\psi \sin \psi \tag{34}$$

$$\hat{Y}_e = \Delta R \sin \psi + R\Delta\psi \cos \psi \tag{35}$$

It was shown in the discussion of figure 25 that these errors were not caused by navigation filter delays. Also shown in figure 31 are the errors due to transition transients when switching between navaids. Figure 31 also presents the altitude error. Note that the altitude error is altitude-dependent. The characteristics of the error changes when blending to MODILS derived altitude. The MODILS altitude error $\hat{Z}_e$ depends on position error ΔR as well as elevation error ΔE.

$$\hat{Z}_e \approx R \tan \Delta E + \Delta R \tan E \tag{36}$$

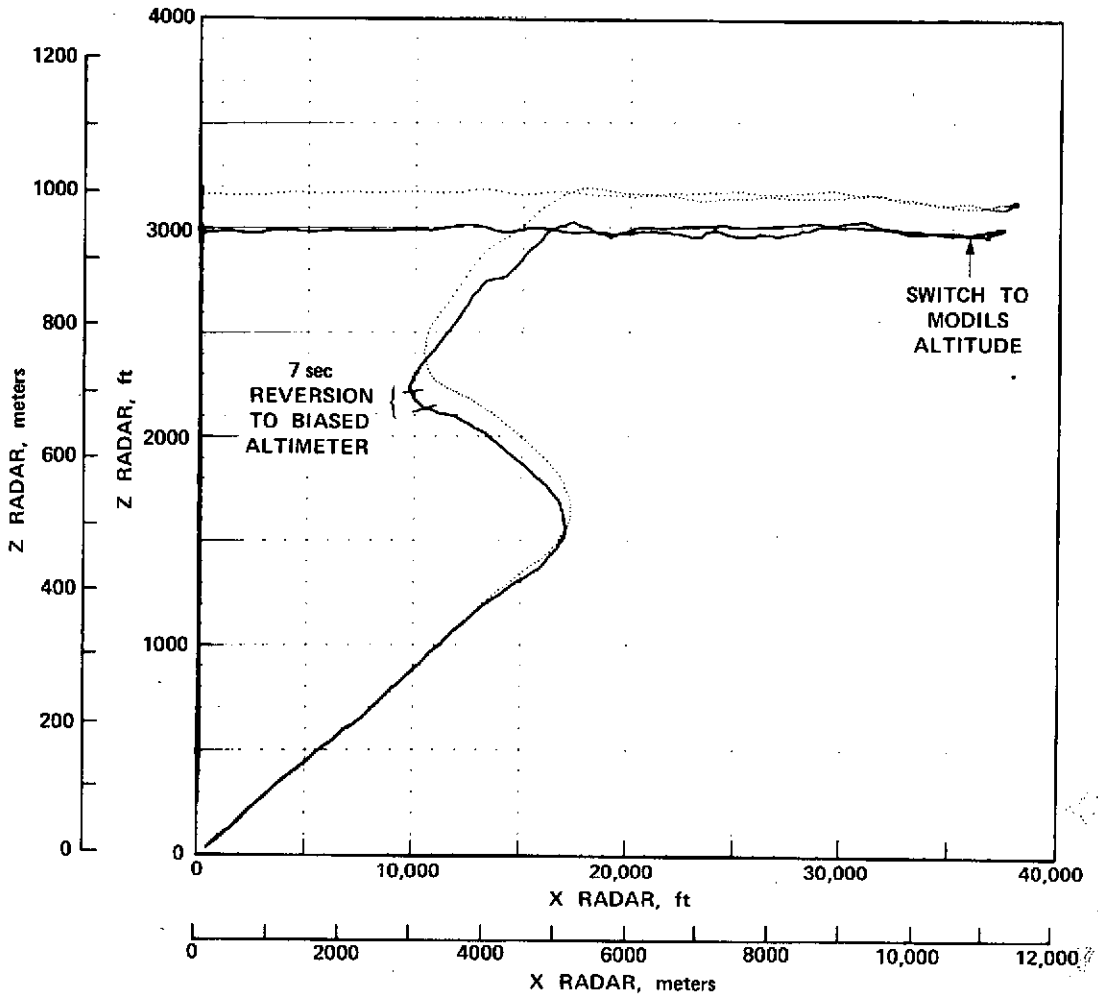

Figure 30.—Portion of vertical flight profile.

that is, the altitude error tends to be larger at higher elevation angles and at further distances from the MODILS landing aid.

The rate errors shown in figure 32 have tendencies following from figure 31. The rate errors center around the average change in position errors (dotted lines) determined from figure 31. Also, the MODILS to TACAN back to MODILS switching transients can be seen. The X and Y rate signals are quite noisy, with error magnitudes as large as wind estimates might be. This is the reason for requiring the large time constant in the wind estimate filters. This concludes the presentation of flight data.

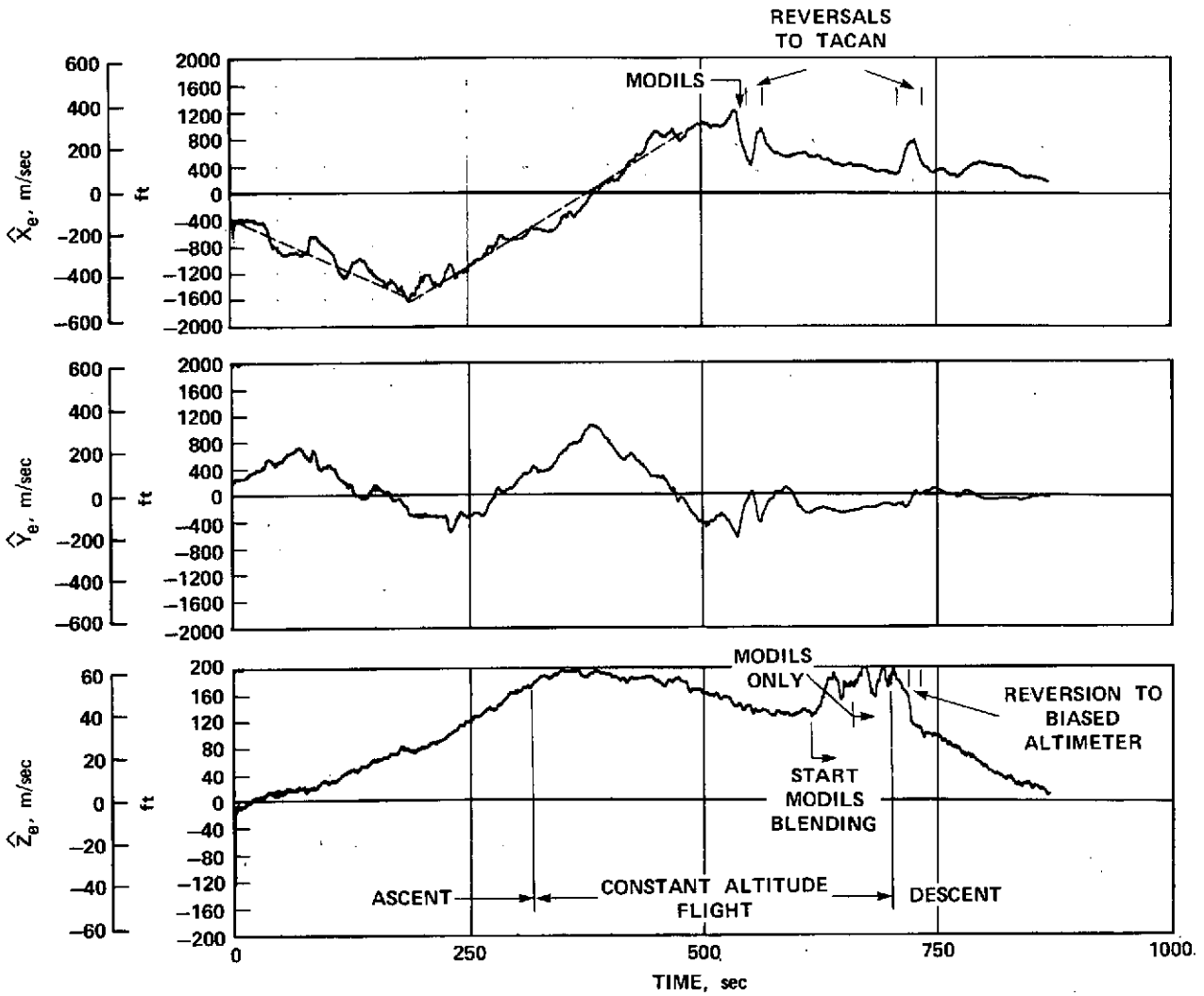

Figure 31.—Navigation errors.

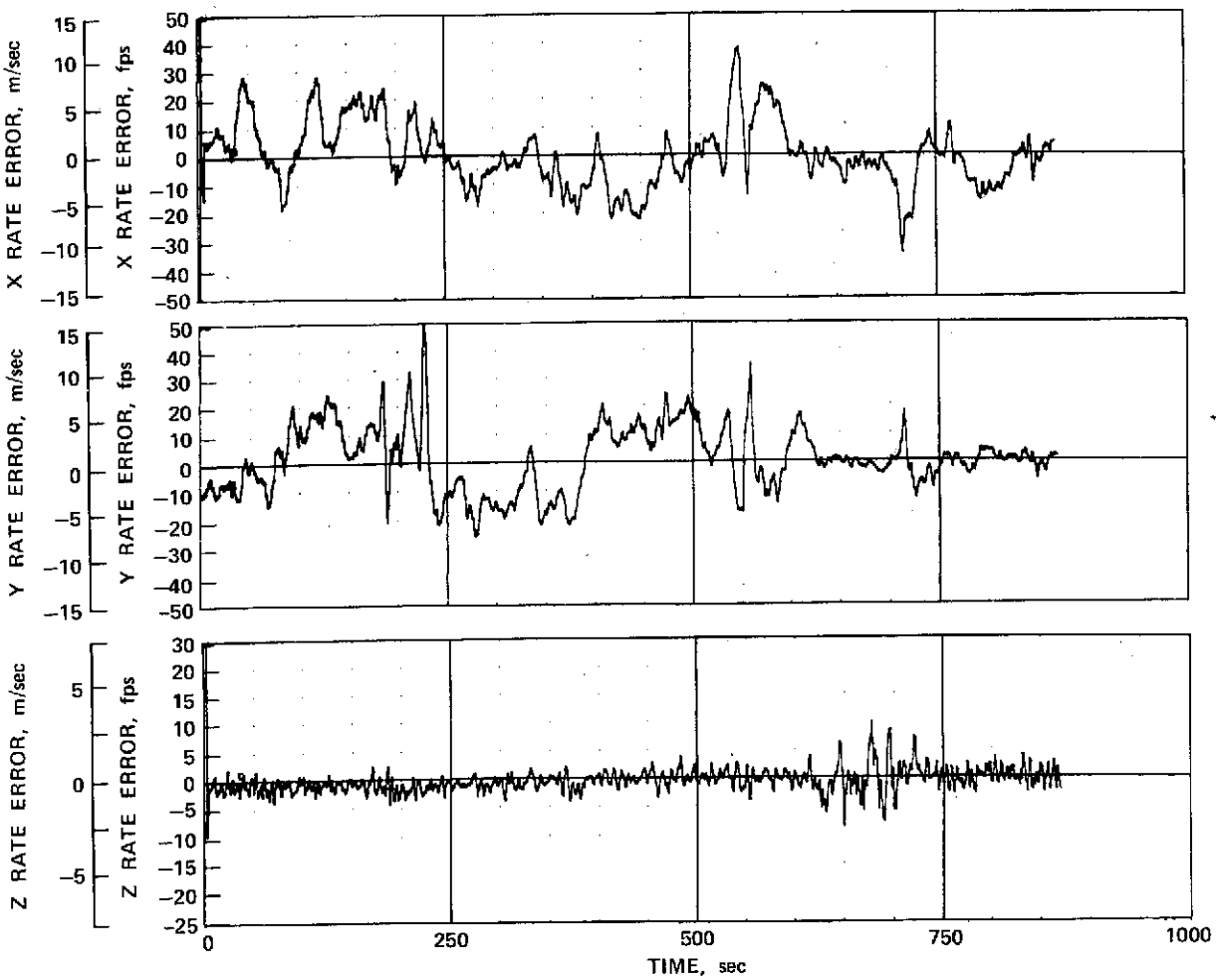

Figure 32.—Navigation rate errors (estimate-radar).

CONCLUDING REMARKS

The mechanization and performance of a terminal area navigation system has been presented. The changes from the basic complementary filter design have been discussed. These changes took care of the input noise characteristics of the DME signals and the switching transient from area to final approach navigation.

Filter gain switching requirements for smooth navigation in the 80 Km radius terminal area have been discussed. Further flight experiments are needed to confirm continuous gain programming as a function of navaid and flight conditions.

It has been pointed out that the system is specialized in map display and navigation computations to one particular airport. To generalize the system so that it is usable in a large geographical region would be a major engineering task. It would mean bulk storage for map data, swapping map data into active storage, changing navaid origins and types, considering a more precise form of cross-country navigation (e.g., multiple DME), and switching to automatic computer-tunable receivers.

REFERENCES

1. S. S. Osder, W. E. Rouse, and L. S. Young, "Navigation, Guidance and Control Systems for V/STOL Aircraft," Sperry Technology, Vol. 1, No. 3, 1973.

2. L. S. Young, Q. M. Hansen, W. E. Rouse and S. S. Osder, "Development of STOLAND, A Versatile Navigation, Guidance and Control System," NASA TMX-62,183, Oct. 1972.

3. G. D. Adams, "Evaluation of STOL Modular Instrument Landing System (MODILS)," National Aviation Facilities Experimental Center, Atlantic City, New Jersey 08405, FAA Department of Transportation. Report No. FAARD-72-4, May 1972.

4. Report of Department of Transportation Air Traffic Control Advisory Committee, Department of Transportation, Washington, D.C., Dec. 1969.

Appendix I

NAVAID NOISE MODELS

TACAN AND VOR/DME NOISE MODELS

The TACAN and VOR/DME stations transmit the clockwise-measured angle from magnetic north to the station. This angle is computed as shown in figure 3. To the computed azimuth, add the noise and bias.

$$\psi_{V/N} = \psi_V + \psi_N + \psi_B$$

Since the TACAN and VOR stations present angles 0 to 360°, when $\psi_{V/N}$ is negative, add 360° to make it a positive angle.

TACAN/VOR Bearing Noise Model

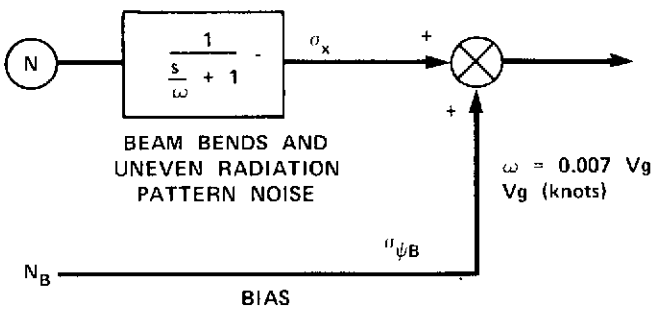

Figure 33.—TACAN bearing noise model.

	TACAN	VOR
σ_ψ	0.1°	0.9°
σ_{ψ_B}	0.59°	0.7°

	TACAN	VOR
$\sigma\psi$	0.1°	0.9°
$\sigma\psi_B$	0.59e	0.7°

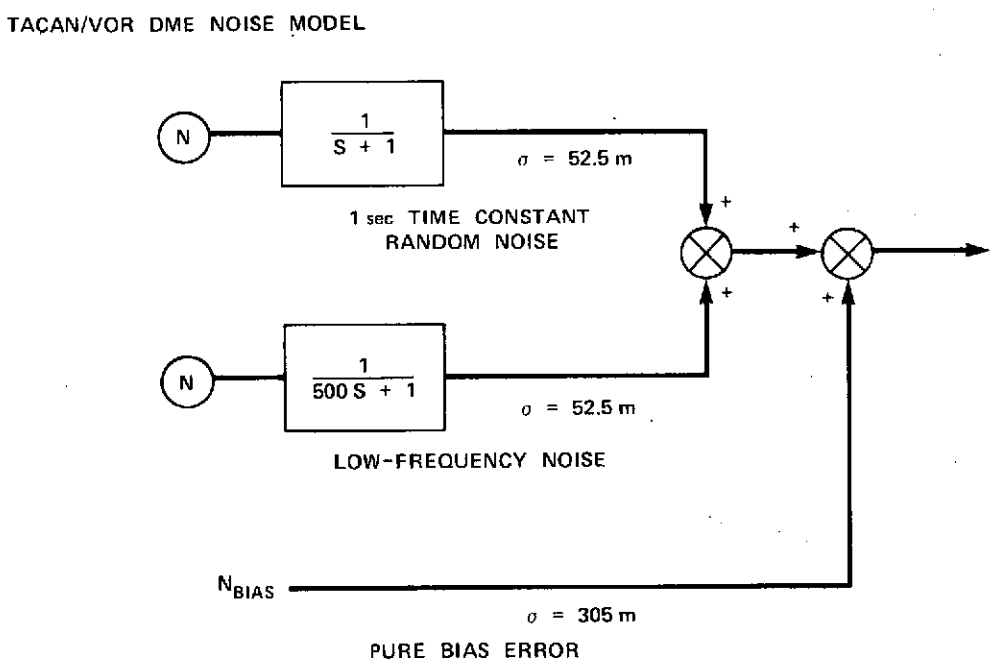

Figure 34.—TACAN DME noise model.

VALIDS

Valids are discrete signals from the navigation receivers to indicate whether the data are to be trusted.

Since TACAN and VOR/DME are line-of-sight systems, the ranges of the systems are smaller for low altitudes

$$\text{Range (n. mi.)} = 1.27 \qquad h \text{ (ft)} = 0.39\ h \text{ (m)}$$

This equation has <u>not</u> been implemented, since we are operating close to the station.

The systems also have a cone of confusion, which is a conical region directly above the station. When the aircraft is inside the conical region, the azimuth valid discrete is set to invalid and incorrect data are transmitted for azimuth.

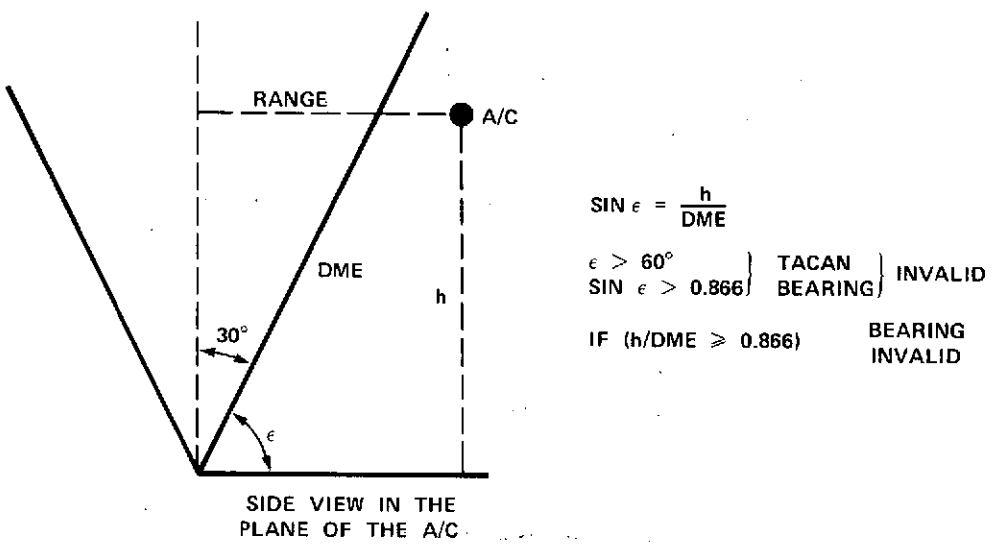

Figure 35.—TACAN cone of confusion.

The DME signal is valid even right above the station. In the STOLAND simulation, all valids can be turned off separately so that the effect of navigation loss on the system can be studied.

MODILS NOISE MODEL

Since MODILS is a scanning beam microwave system, it is thought that noise on sequential samples is not correlated. To each signal that is calculated as shown in figure 4, both noise and bias errors are added.

$$DME_{+N} = DME + DME_{bias} + N_{DME}$$

$$\psi_{+N} = \psi_c + \psi_{bias} + N_{\psi}$$

$$\varepsilon_{+N} = \varepsilon_c + \varepsilon_{bias} + N_{\varepsilon}$$

The statistics of the bias and random noise quantities are:

Quantity	Standard deviation of Gaussian distributions
DME_{bias}	6.1 m
ψ_{bias}	0.17°
ε_{bias}	0.05°
$\sigma_{N_{DME}}$	12.2 m
$\sigma_{N_{\psi}}$	0.03°
$\sigma_{N_{\varepsilon}}$	0.07°

It should be noted that the noises in the MODILS system installed at Crows Landing are somewhat larger and have a more complex structure, as discussed in reference 3. A complete implementation on the 8400 computer is not possible due to time and storage limitations.

Appendix II

SENSOR SPECIFICATIONS

TACAN RECEIVER/TRANSMITTER

MADE BY : Hoffman Nav Com Systems
MODEL NO. : RT 1057/ARN-103
PART NO. : 8010000083-11

CHARACTERISTIC	SPECIFICATION
Power input	115 Vac, 400 Hz, 375 W (max. with blower) 26 Vac, 400 Hz, 20 W 28 Vdc, 62 W
Frequency	1025 - 1150 MHz transmitter 962 - 1213 MHz receiver
Channels	126, X-mode - 126, Y-mode
Channeling time	Less than 1 sec max
Range	0 to 300 n. mi.
Sensitivity	-90 dBm min
Power output	1.5 kW nom, 4.0 kW max
Digital outputs	ARINC 582 and ARINC 568 serial outputs
Digital accuracy	Range: ±0.05 n. mi. 0 to 50 n. mi. ±0.10 n. mi. 50 to 300 n. mi. } from 0 to -90 dBm Bearing: ±0.5° from 0 to -82 dBm
Digital resolution	Bearing: ±0.25°
Analog outputs	ARINC 582 range and bearing outputs for HSI and BHDI indicators
Analog accuracy	Range: ±0.10 n. mi. 0 to 50 n. mi. ±0.15 n. mi. 50 to 300 n. mi. } from 0 to -90 dBm
Analog resolution	Bearing: ±0.4° (approx.)
Dynamic tracking	0 to 4500 knots of ground speed
Speed of response	3 to 8 sec (max)
Weight	19.5 kg

DME DISTANCE MEASURING EQUIPMENT

MADE BY : Collins Radio Company
MODEL NO. : 860E-3
PART NO. : 522-4209-001

CHARACTERISTIC	SPECIFICATION
Power input	115 Vac, 400 Hz, 89 W (nom. with blower)
Frequency	1025 - 1150 MHz transmitter 962 - 1213 MHz receiver
Channels	126, X-mode - 126, Y-mode
Channeling time	400 ms nom
Range	0 to 390 n. mi.
Sensitivity	-93 dBm nom
Power output	30 ±3 dBW
Digital outputs	Per ARINC 568
Analog outputs	Per ARINC 568

Accuracy

Distance (n. mi.)	Signal Level (dBm)	Fixed Speed (kn)	Error (n. mi.)
0 to 5	-20 to -60	0 to 200	±0.1
0 to 5	-60 to -80	0 to 200	±0.2
5 to 380	-20 to -80	0 to 2000	±0.2
5 to 380	lock onto -80 dBm	0 to 2000	±0.4

Dynamic tracking	0 to 2000 knots
Memory	4 to 12 sec
Weight	8.62 kg

VOR/ILS RECEIVER

MADE BY : Collins Radio Company
MODEL NO. : 51RV-2B
PART NO. : 522-4280-107

CHARACTERISTIC	SPECIFICATION
Power input	VOR: 27.5 Vdc, 40 W; 26 Vac, 400 Hz, 16 VA ILS: 27.5 Vdc, 44 W; 26 Vac, 400 Hz, 16 VA
Frequency	VOR: 108 to 118 MHz (even tenths MHz only from 108 to 112 MHz) LOC: 108 to 112 MHz (odd tenths MHz only) G/S: 329.3 to 335.0 MHz
Channels:	VOR: 180 LOC: 20 G/S: 20
Channel increments	VOR: 50 kHz LOC: 200 kHz G/S: 300 kHz
Channeling time	1 sec or less
Output circuits:	
VOR/LOC deviation	Five 1000-ohm loads; 150 μa/10° VOR, 90 μA/4 dB LOC.
G/S deviation	Five 1000-ohm load capability
To/from	650 μA/load - two 200-ohm load capability
VOR/LOC flag	(High level) 27.5 Vdc 250 mA (Low level) four 1000-ohm load capability
G/S flag	(High level) 27.5 Vdc 250 mA (Low level) four 1000-ohm load capability
Accuracy	
VOR	Less than ±1.0°. RMI card servo amp null width is less than ±0.5°.
LOC	Less than ±2 μA centering
G/S	Less than ±3 μA centering
Weight	8.35 kg

RADIO ALTIMETER

MADE BY : Bendix Avionics Division
MODEL NO. : ALA-51
PART NO. : 2067631-5151

CHARACTERISTIC	SPECIFICATION
Power input	115 Vac, 400 Hz, 85 VA
Frequency	4.2 to 4.4 GHz
Deviation	140 MHz
System type	FM/FM/CW
Antenna	Dual horns
Beamwidth	Roll 50 ±5° - pitch 40 ±5°
Range	-20 to 2500 feet altitude
Step error	Less than 1/2-foot
Doppler error	None
Pitch limits	±20°
Roll limits	±30°
Power output	400 mW
Analog output	0.4 Vdc +0.02 Vdc per foot
Analog accuracy	0 to 100 feet = ±1.5 feet (per ARINC 552A) 0 to 500 feet = ±2.0 feet or 2% 500 to 2500 feet = ±3%
Trip signals	6 - shop adjustable 1 - pilot adjustable
Trip signal accuracy	Shop set: 0 to 500 feet = ±3 ft. or 3% 500 to 2500 feet = ±6% Pilot Set: 0 to 500 feet = ±3 ft. or 3% 500 to 2500 feet = ±5%
Weight	8.03 kg

MODILS AIRBORNE RECEIVER/TRANSMITTER

MADE BY : Raytheon Co., Inc.
MODEL NO. : None
PART NO. : 1689

CHARACTERISTIC	SPECIFICATION	
Power input	28 Vdc, 3.0 A	
Frequency	5.185 ±0.01 GHz transmitter	
	5.20 to 5.24 GHz receiver	
Channels	20	
Channeling time	1.5 sec	
Nominal range	80,467 m (±25° from runway C/L)	
Outputs	Azimuth:	BCD 00.0° to 99.9° (45.0° centerline)
	Elevation:	BCD 00.0° to 19.99°
	Range:	0.00 to 16,077 m (ARINC 568 characteristic)
Usable coverage	Azimuth:	±21.4° (from runway C/L)
	Elevation:	1.96° to 16.44°
	Range:	161 to 16,077 m
Accuracy	Azimuth:	±0.25°
	Elevation:	±0.07°
	Range:	±0.01 mile ±1% of range
Weight	8.62 kg	

PITCH RATE GYRO

MADE BY	:	Northrop Corporation, Electronics Division
MODEL NO.	:	
MFG. PART NO.	:	
SPERRY PART NO.	:	4007048-902

CHARACTERISTIC	SPECIFICATION
Power input	26 Vac, 400 Hz, 200 mA 35 Vac, 400 Hz, 2 mA +28 Vdc 50 mA ±15 Vdc
Range	40°/sec
Scale factor	125 mV/°/sec
Threshold	0.04°/sec (max)
Resolution	0.04°/sec (max)
Zero Offset	0.10°/sec (max)
Linearity	±0.5% of fullscale to half-scale ±2.0% to fullscale
Hysteresis	0.06°/sec
Static balance	0.05°/sec/g (max)
Null	25 mV rms
Natural frequency	23 Hz (min)
Damping ratio	0.5 to 1.0
Output signal range	0 ± 10 Vdc analog
Rate signal scaling	0.25 Vdc/°/sec
Weight	0.64 kg

YAW/ROLL RATE GYRO

MADE BY : Northrop Corporation, Electronics Division
MODEL NO. :
MFG. PART NO. :
SPERRY PART NO. : 4007048-901

CHARACTERISTIC	SPECIFICATION
Power input	26 Vac, 400 Hz, 400 mA 35 Vac, 400 Hz, 4 mA +28 Vdc 50 mA ±15 Vdc
Range	40°/sec
Scale factor	125 mV/°/sec
Threshold	0.04°/sec (max)
Resolution	0.04°/sec (max)
Zero offset	0.10°/sec (max)
Linearity (% of fullscale)	±0.05% to halfscale ±2.0% to fullscale
Hysteresis	0.06°/sec
Static balance	0.05°/sec/g (max)
Null	25 mV rms
Natural frequency	23 Hz (min)
Damping ratio	0.5 to 1.0
Output signal range	0 ± 10 Vdc
Rate signal scaling	0.25 Vdc/°/sec
Weight	0.79 kg

Note: Power input shown is the total power required by the yaw/roll rate gyro assembly. All other specifications are identical for both yaw and roll rate gyros in the assembly.

3-AXIS ACCELEROMETER ASSEMBLY

MADE BY : Sperry Flight Systems*
MFG. PART NO. : 4006992

CHARACTERISTIC	SPECIFICATION	
Power input	±15 Vdc, 60 mA per accelerometer	
	Normal	Lateral/Longitudinal
Range	-1 to +4 g	0 ± 1 g
Scale factor (100K external load)	2 Vdc/g (0 V @ +1 g)	5 Vdc/g
Scale factor tolerance @ 25° C	±0.25%	±0.25%
Null @ 25° C	0.015 g	0.0016 g
Scale factor change with temperature	±0.018%/° C	±0.018%/° C
Null change with temperature	±0.0006 g/° C	±0.0006 g/°C
Hysteresis	±0.0008 g	±0.0002 g
Cross axis sensitivity	±0.002 g/g	±0.002 g/g
Natural frequency	>50 Hz	>50 Hz
Case alignment	±0.25°	±0.25°
Weight	0.48 kg for complete assembly	

*Assembly contains three accelerometers manufactured by Systron Donner: Normal = model 4384A-4-P5, Sperry part no. 4010677-1; Lateral/longitudinal = model 4384A-1-P6, Sperry part no. 4010677-2.

STATIC PRESSURE SENSOR

MADE BY : Sperry Flight Systems
MODEL NO. : None
PART NO. : 4009996

CHARACTERISTIC	SPECIFICATION
Power input	+15 Vdc, 400 mA
	-15 Vdc, 50 mA
Range	0 to 35 in. Hg
Overpressure limit	150% of normal range
Output range	1 to 4 kHz
Resolution	Better than 0.0001 in. Hg
Accuracy (3)	0.003 in. Hg +0.02% of pressure in in. Hg with output frequency corrected for sensor temperature
Hysteresis	Less than 0.003 in. Hg
Temperature sensitivity	Linear from 0.006 in. Hg/° C at 30 in. Hg to zero in. Hg/° C at 1.0 in. Hg. (Constant 0.0002/° C times reading in in. Hg.)
g-sensitivity	0.010 in. Hg/g acceleration (normal axis of diaphragm)
	0.001 in. Hg/g acceleration (tangent axis of diaphragm)
Temperature sensor output voltage as function of T	Typical - linear over range
Weight	1.22 kg

DIFFERENTIAL PRESSURE SENSOR

MADE BY : Rosemount Engineering Co.
MODEL NO. : 1221 A-3G10BC
MFG. PART NO. : None
SPERRY PART NO. : 4010482

CHARACTERISTIC	SPECIFICATION
Input power	+15 Vdc ±10%, 40 mA
	-15 Vdc ±10%, 40 mA
Design pressure range	0 to 5 in. Hg
Resolution	±0.1% of design pressure span
Repeatability	±0.02% of design pressure span
Hysteresis	±0.015% of design pressure span
Temperature error:	
0 to +50° C	±0.50% of calibrated pressure span over full design pressure range
-55 to +71° C	±1.0% of calibrated pressure span over full design pressure range
Response time	25 ms nom.
Output scale factor	Linear 2.5 Vdc/in. Hg into 100K load
Weight	0.37 kg

TOTAL TEMPERATURE SENSOR

MADE BY : Rosemount Engineering Co.
MODEL NO. : 101-AA MIL Type MA-1
MFG. PART NO. : None
SPERRY PART NO. : 4010670

CHARACTERISTIC	SPECIFICATION
Range:	
Temperature	-70° C to +350° C
Mach	0 to 3 Mach
Altitude	0 to 30,000 m
Power source	1.2 mA at 28 Vdc
Resistance vs temperature	$R_t/R_o = 1 + \alpha/T - \delta(T/100 - 1)(T/100) - \beta(T/100 - 1)(T/100)^3$ R_t = resistance in ohms at temperature T R_o = 500 ohms T = temperature in °C α = 0.003925 δ = 1.45 β = 0 for +T; 0.1 for -T
Accuracy	Less than 0.25° C + 0.5% of the magnitude of temperature in °C.

VERTICAL GYRO

MADE BY : Sperry Flight Systems
MODEL NO. : VG-321
PART NO. : 2587335-21

CHARACTERISTIC	SPECIFICATION
Power input	115 Vac, 400 Hz, 115 VA, 60 W (max start) 115 Vac, 400 Hz, 60 VA, 25 W (max run)
Rotor speed	11,000 rpm (nom.)
Angular momentum	4 million g cm^2/sec
Verticality	±.375° (level unaccelerated flight)
Erection rates	Roll: Fast, 33°/min (nom.) Slow, 2.1°/min (nom.) Pitch: Fast, 12°/min (nom.) Slow, 2.1°/min (nom.)
Erection cut-off threshold	0.10 g lateral 0.04 g longitudinal
Roll and pitch	3-wire synchro 0.205 Vac/°
Signal outputs	2-wire flights director 0.205 Vac/° 2-wire radar, 0.050 Vac/° 2-wire spare, 0.050 Vac/°
Weight	6.71 kg